FOR REFERENCE

NOT TO BE TAKEN FROM THIS ROOM

STUDY OF LOW-FREQUENCY NOISE IN AMORPHOUS SILICON

by

İ. HAKAN PEKCAN

B.S. in E.E., İstanbul Technical University, 1983

Submitted to the Institute for Graduate Studies in Science and Engineering in Partial Fulfilment of the requirements for the degree of

Master of Science

in

Electrical Engineering

Bogazici University Library
39001100313280
14

Boğaziçi University

1987

ACKNOWLEDGEMENTS

I wish to express my sincere gratitute to Doç. Dr. Yekta ÜLGEN, my thesis supervisor, who was a constant source of guidance, support and valuable suggestions throughout the preparation of this thesis.

The encouragement, help and thoughtfulness of Y. Doç. Dr. Gülen AKTAŞ in providing me with working facilities in the Solid State Physics Laboratory - a really stimulating and friendly environment - are sincerely acknowledged.

ABSTRACT

In this thesis, amorphous silicon films are fabricated and their low-frequency noise properties are investigated over the range of 10 Hz to 4.4 kHz. The ohmic contacted films are produced in two different geometries using the electron gun vacuum-evaporation technique. The noise measurements carried out at low-frequencies show that, 1/f noise is dominant in this frequency region. Effects of d.c. biasing and increasing ambient temperature are also investigated; increasing temperature ($> 300\ ^{o}K$) decreases the low-frequency noise power level. The relationship between the hopping rate and the 1/f noise is verified. It is also shown that, the density of states near the Fermi level can be calculated from 1/f noise measurements. Amorphous silicon films are found to be noisier than the crystalline structure.

ÖZETÇE

Bu çalışmada, amorf silisyum filmler oluşturdukları gürültü açısından incelenmiştir. Omik kontaklı olan filmler vakumda elektron tabancası ile buharlaştırılarak iki farklı geometride gerçekleştirilmiştir. 10 Hertz'den 4.4 kHz'e kadarlık bir frekans ekseni boyunca gürültü spektrumu belirlenmiş ve bu frekans bölgesindeki ölçümler 1/f tipi karakteristiğin geçerli olduğunu göstermiştir. Ölçümlerde doğru akım kutuplama gerilimi ve sıcaklık değiştirilerek etkin gürültü direnci belirlenmiştir. Artan sıcaklıklarda (>300°K) gürültü seviyesinin azaldığı görülmüştür. Oda sıcaklığında fonon yardımlı atlama olayı ile gürültü oluşumu arasında ilişki kurulmuş ve bu bölgede Fermi seviyesi durum yoğunluğunun, gürültü ölçme yöntemiyle hesaplanabileceği gösterilmiştir. Ayrıca, amorf olmayan silisyum kristalinin gürültüsü de ölçülerek, amorf silisyumdan daha gürültülü olduğu gözlenmiştir.

TABLE OF CONTENTS

	Page
ACKNOWLEDGEMENTS	iii
ABSTRACT	iv
ÖZETÇE	v
TABLE OF CONTENTS	vi
LIST OF FIGURES	viii
INTRODUCTION	1
CHAPTER 1- THEORY OF AMORPHOUS SOLIDS	3
1.1. Physical Structure of Amorphous Solids	3
1.2. Electrical Properties of Amorphous Semiconductors	7
1.2.1. Different Conduction Mechanisms	7
1.2.2. D.C. Conductivity	8
CHAPTER 2- NOISE CONSIDERATIONS AND LOW-FREQUENCY NOISE	12
2.1. The Noise Phenomena	12
2.2. The Low-Frequency Noise in Conductors	13
2.3. Noise Generation Mechanism in Amorphous Silicon	16
2.4. Narrow-Band Noise Detection	18
2.4.1. Noise in a Narrow-Band Filter	19
2.4.2. True rms to dc Conversion in Noise Measurements	22

CHAPTER 3- EXPERIMENTAL TECHNIQUES 28

3.1. Preparation of the Samples 28

3.2. Measuring Equipment 32

3.3. 1/f Noise With D.C. Excitation 34

3.3.1. Theoretical Considerations 34

3.3.2. Summary of Experimental Results 38

CHAPTER 4- CONCLUSIONS 54

REFERENCES 56

LIST OF FIGURES

FIGURE 1.1. Models for the Distribution of the Density of Localized States,

a) Cohen, Frizsche, Ovshinsky (CFO) Model, 1969.

b) Davis and Mott Model, 1970.

FIGURE 2.1. The schematic of the Set-up Used for the Measurement of Noise Power Spectrum.

FIGURE 2.2. Power Spectral Density in a Narrow-Band Filter.

FIGURE 2.3. Input and Output of the Narrow-Band Filter.

FIGURE 2.4. A True rms Converter Proposed for Noise Measurements.

FIGURE 2.5. True rms to dc Converter.

FIGURE 3.1. Masks Used in the Preparation of Coplanar Geometry Samples,

a) Silicon Mask

b) Electrode Mask

c) Cross-section of the Prepared Film in Coplanar Geometry

FIGURE 3.2. The Preparation of Sandwich Type Samples,

a) Masks

b) TopView of the Prepared Film

c) Cross-section of the Prepared Film in Sandwich Geometry

FIGURE 3.3. D.C. biasing of the amorphous silicon samples.

FIGURE 3.4. Equivalent noise circuit with sandwich type samples.

FIGURE 3.5. Equivalent representation of the amplifier by its noise sources with noise-free amplifier.

FIGURE 3.6. System Noise Characteristics.

FIGURE 3.7. Typical I-V Curve of a Sample at Room Temperature.

FIGURE 3.8. Typical C versus f Graph of a Sandwich Type Sample.

FIGURE 3.9. Low-Frequency Noise of the Sandwich Sample no.1

FIGURE 3.10. Low-Frequency Noise of the Sandwich Sample no.2

FIGURE 3.11. Low-Frequency Noise of the Coplanar Sample no.1

FIGURE 3.12. Low-Frequency Noise of the Coplanar Sample no.2

FIGURE 3.13. Low-Frequency Noise of the Coplanar Sample no.3

FIGURE 3.14. Effective Noise Resistance versus V_{dc}^2 Graph of a Sandwich Sample.

FIGURE 3.15. Effective Noise Resistance versus V_{dc}^2 Graph of a Coplanar Sample.

FIGURE 3.16. Low-Frequency Noise in a Crystalline Silicon Film.

FIGURE 3.17. Temperature Dependence of the Low-Frequency Noise for a Coplanar Sample.

FIGURE 3.18. Effective Noise Resistance versus V_{dc}^2 Graph at High Temperature (400^oK).

INTRODUCTION

Amorphous semiconductors have gained a vast popularity during the last decade; interests in both theoretical and experimental aspects have grown at an enormous rate.

Amorphous materials are cheap and easy to produce, the electrical properties of them can easily be changed by doping or hydrogenating. As a matter of fact, some electronic components, such as solar cells, diodes and field effect transistors, can be constructed using amorphous materials.

However, there is a very little done on low-frequency noise measurements of amorphous silicon. The existence of 1/f type spectrum has been experimentally checked and the low-frequency noise power is investigated both as a function of temperature and d.c. applied bias. It is also possible to use low-frequency noise measurements for the reliability assesment of amorphous samples.

The amorphous silicon samples used in noise experiments are all prepared in Solid State Physics laboratory and because of limited equipment facilities it has not been possible to hydrogenate these samples.

There is not much work done on the temperature dependence of 1/f noise in amorphous silicon, hence this would be an interesting topic of research for future work.

CHAPTER I
THEORY OF AMORPHOUS SOLIDS

1.1. PHYSICAL STRUCTURE OF AMORPHOUS SOLIDS

Crystalline materials having the ideal periodic structure are characterized as periodic array of atoms, with short-range and also long-range coordination. This means that the environment of an atom chosen at random is precisely the same, no matter how far away it is examined, as the environment of any other atom. On the contrary, the introduction of various types of defects and impurities results in deviations from the ideal structure.

Electron and x-ray diffraction results have shown that amorphous materials exhibit a high degree of short range order [1]. Despite the fact that nearest neighbour environments in amorphous materials are precisely the same as in the crystalline material, they have no long-range order. Randomly distributed atoms, from the long-range viewpoint, cause an imperfection called positional disorder. Consequently it can be said that because of the lack of long-range periodicity it is much more difficult to determine the structure in amorphous materials.

On the other hand, internal voids and dangling bonds are the symptoms of defects of another kind, Amorphous materials contain many voids within the structure (the so-called "Swiss cheese model"). These voids lead to interior dangling bonds and they can dominate the electrical properties of the material. This type of defects in amorphous semiconductors result from strain-relief mechanism and from bonding misfits during the growth process [2].

The properties of amorphous films depend strongly on the preparation methods. Amorphous slicon (a-Si) films are commonly obtained by one of three basic methods. These are,

1. Vapour deposition (Vacuum Evaporation)
   a. Thermal Evaporation
   b. Electron Gun Evaporation
2. Sputtering
3. Glow-discharge decomposition of silane (SiH_4)

The samples prepared by glow-discharge silane have fewer voids and dangling bonds compared to those prepared by evaporation or sputtering techniques [3,4,7]. It is likely that an a-Si film formed by glow-discharge method contains residual hydrogen which tends to saturate the potential dangling bonds.

The films have heterogeneous structure when they are deposited on a sufficiently cold substrate by evaporation or sputtering. Accordingly, they contain voids and dangling bonds causing a structural disorder.

It should be noted that amorphous semiconducting films cannot be obtained by rapid quenching from the melt. Therefore bulk amorphous material has not yet been produced.

In a crystalline material high mobilities of free (delocalised) carriers can be expressed by the Bloch theorem which is an implication of periodicity. But an amorphous solid, unlike the crystal, with the disorder present does not follow this theorem; thus many of the results derived for crystals do not apply directly to amorphous materials [8]. Similarly, the electron wave function and some other particular concepts determining the periodicity of a crystal lattice are no longer applicable to amorphous solids owing to the absence of periodicity. However, other ideas developed for crystals remain valid even in disordered states.

When dealing with the band structure of crystalline semiconductors, impurity energy bands in the forbidden gap are of prime importance. These narrow and continuous impurity energy bands constitute localized energy states, namely donor and acceptor energy levels closer to conduction band and valance band respectively. In contrast, lack of long-range periodicity and defects in the amorphous semiconductors result in a continuous distribution of localized states in the energy gap. The mobility of charge carriers in an amorphous solid sensitively depends on the density of states N(E). Thus the conduction mechanisms can be explained by means of the distribution of the density of localised states.

In order to describe the conduction mechanisms in amorphous semiconductors, Cohen, Fritzsche and Ovshinsky (CFO) in 1969; Davis and Mott in 1970 proposed two different band models [5,6]. These models are sketched in Figure 1.1 where the shaded areas represent the localized states.

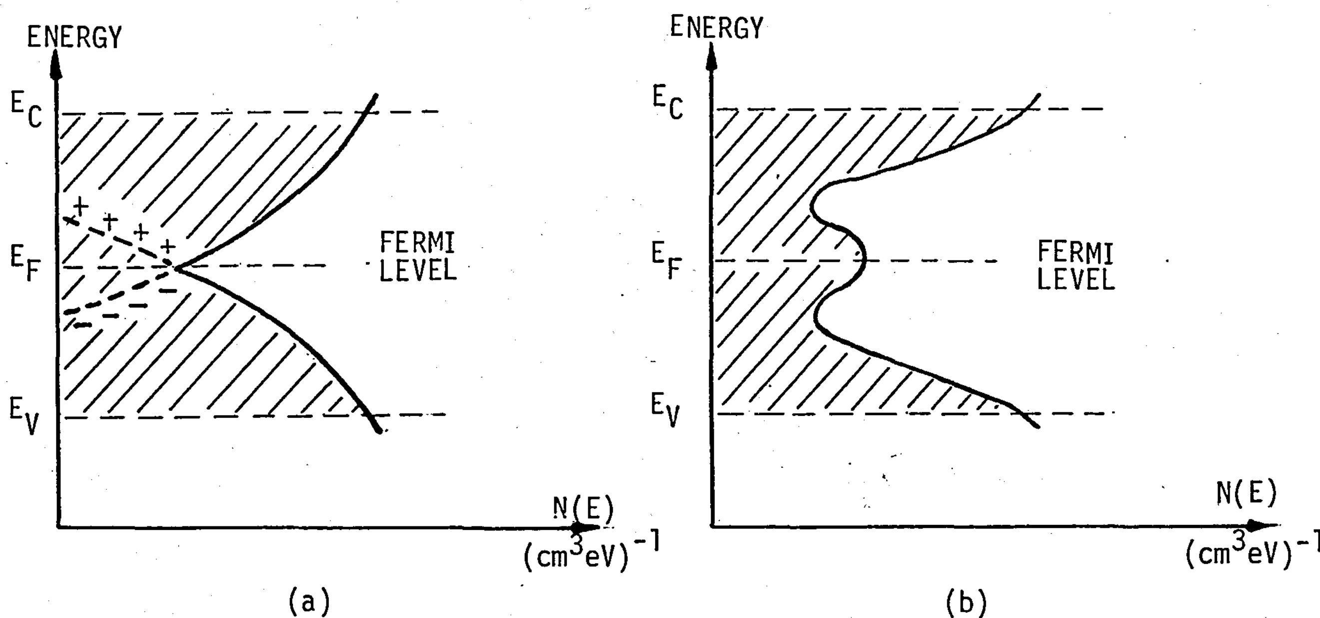

FIGURE 1.1

Models for the Distribution of the Density of Localized States

(a) Cohen, Fritzsche, Ovshinsky (CFO) Model, 1969

(b) Davis and Mott Model. 1970

The density of states does not vanish anywhere in the energy gap. These states extend into the gap from both conduction and valence bands. A stronger distinction is made between localized states; the localized states near the band edges originate from the lack of long-range order, but the localized states near the middle of the gap are due to dangling bonds.

Common to all suggested models are the critical energies (mobility edges) E_c and E_v which separate the localized states in the mobility gap from band states. Another common feature of these models is that there is a finite density of localized states at the Fermi energy level.

In the CFO model, tails of localized states extend from the valence and conduction bands into the energy gap. These overlapping states moreover lock the Fermi level near the middle of the band. The tail from the conduction band consists of donors and the tail from the valance band of acceptors. Hence repopulation occurs and the higher acceptor states give up electrons to the lower donor states. This cause the creation of large concentration of positively and negatively charged centers or traps. These donor like and acceptor like states effectively determine the Fermi level.

In the Davis and Mott model, the tails of localized states do not overlap. Fermi level is the maximum value of the density of localized states near the middle of the gap.

1.2 ELECTRICAL PROPERTIES OF AMORPHOUS SEMICONDUCTORS

1.2.1 Different Conduction Mechanisms

Different conduction mechanisms are to be expected owing to the different properties of electron states in and out of the mobility gap. In the extended states, almost normal carrier mobility of about 1 to 10 $cm^2/V.sec$ is considered. But in the localized states Phonon Assisted Tunneling is the dominant transport mechanism [9]. The transition from the extended to localized states at conduction band edge (E_c) and valance band edge (E_v) cause the abrupt drop of mobility. As explained in the previous section, CFO model suggests that the valance and conduction band tails actually overlap in the energy gap. Such a situation preserves a gap between the mobility edges and it is the existence of this mobility gap as a pseudo gap, (E_c-E_v).

Consequently, depending on the ambient temperature, two different conduction mechanisms are concerned. In the extended state conduction at high temperatures, the electrons are excited to the conduction band and holes to the valance band. At low temperatures the conductivity mechanism is dominated by phonon assisted hopping in the regions of localized states.

1.2.2. D.C. Conductivity

There are four different types of conduction mechanisms in a-Si. These mechanisms are investigated using the models given in the first section.

1. Conduction in the extended states near the Mobility Edge,

If the Fermi energy lies in a region of strongly localized states, the current may be carried by electrons excited to the mobility edge. In this case the conductivity for electrons is,

$$\sigma = \sigma(E_c)\ \exp(-\Delta E/kT) \tag{1.1}$$

where $\Delta E = E_c - E_F$

$$\sigma(E_c) = kTq\mu N(E_c) \tag{1.2}$$

Taking the Neperial logarithm of both sides in Equation (1.1),

$$\ln\sigma = \ln(\text{constant}) - \Delta E/kT$$

and

$$\frac{\Delta \ln \sigma}{\Delta(1/T)} \sim - \frac{\Delta E}{k} \tag{1.3}$$

According to the above equation one can plot $\ln \sigma$ versus 1/T characteristics to give a straight line and determine $\Delta E/k$ as the slope.

Near the edge of the conduction band, the metallic conductivity is minimum,

$$\sigma_{min} = 26.10^{-3} \frac{q^2}{\hbar a} [\Omega \mathrm{cm}]^{-1} \tag{1.4}$$

where a is the interatomic spacing.

2. Conduction by carriers excited into the localized states at the band edges and hopping at energies E_x;

For this process, assuming again conduction by electrons, the conductivity is written as

$$\sigma = \sigma_x \exp\left[-(E_x - E_F + W_x)/kT\right] \tag{1.5}$$

Where E_x is the energy level in the localized state region near the conduction band edge, W_x is the activation energy for hopping at energy E_x and σ_x is the pre-exponential factor.

3. At room temperature and below temperatures transport is dominated by hopping of electrons through defect states at the Fermi level [5].

If the density of states at E_F is finite, there will be a contribution from carriers which can hop between localized states. Here, at least three factors influence the hopping process and then the probability of jumping from one site to another is

$$p = \nu \exp(-2\alpha R - W/kT) \tag{1.6}$$

where ν is the phonon frequency, α is the rate of decay of the localized wave function, R is the hopping distance between two sites and W is the activation energy for hopping near the Fermi level. Then, the conductivity in terms of Hopping to nearest neighbours (HNN) is

$$\sigma_{HNN} = \sigma_{OHNN}(\exp -W/kT) \tag{1.7}$$

where σ_{OHNN} is the pre-exponential factor.

4. At sufficiently low temperatures, such as kT less than the bandwidth of Fermi energy, the phenomenon of "Variable Range Hopping (VRH)" is expected instead of nearest neighbour hopping [5,6].

Conductivity related to this mechanism is given by Mott's well-known formula;

$$\sigma_{VRH} = \sigma_{VRH}(T) \exp(-T_o/T)^{1/4} \tag{1.8}$$

where T_o is a constant in connection with the density of states at the Fermi level $N(E_F)$ in the following way,

$$T_o = \frac{19,6\ \alpha^3}{kN(E_F)} \tag{1.9}$$

In this temperature range, $\ln \sigma$ versus $T^{-1/4}$ graph can be given. The slope of this graph gives $N(E_F)$ value.

On the other hand, the mechanisms that can be given for D.C. conductivity all contribute to the A.C. conductivity. Obviously these mechanisms of charge transport result in frequency dependent conductivity.

CHAPTER II

NOISE CONSIDERATIONS AND LOW-FREQUENCY NOISE

2.1. THE NOISE PHENOMENA

Noise, in general, can be described as any unwanted disturbance that obscures or interferes with a desired signal. Disturbances coming from external sources called man-made noise and they can be eliminated by suitable methods. Here, this type of noise is out of interest such that we use the word "noise" to represent basic random noise generation and spontaneous fluctuations which result from the physics of the devices and materials making up the electrical system.

The random character of noise makes it impossible to predetermine precisely what the instantaneous value of these fluctuations will be. It consists of frequency components that are random in both amplitude and phase. Although the average value is zero, the long-term rms value can be measured. Accordingly, the rms noise voltage given as,

$$v_{n_{rms}} = \left(\frac{1}{T} \int_0^T v_n^2(t)dt \right)^{1/2} = (\overline{v_n^2})^{1/2} \qquad (2.1)$$

is important in noise measurements.

The noise mechanisms can be classified in three main groups:

1. Thermal noise (White noise)

2. Shot noise

3. Low-frequency noise (1/f noise, burst noise, pop-corn noise)

The most often encountered type is thermal noise. This type of noise is generated by conductors (or resistors) due to thermally activated random motions of electrons.

Shot noise is always associated with p-n junctions. This is due to the fluctuations in the carrier energies causing current fluctuation.

Low frequency noise, as the name implies, dominates the low-frequency end of the spectrum. In this frequency region spectral noise density function increases according to the 1/f rule. Noise with an approximately 1/f frequency spectrum is found nearly in all current carrying electronic devices. In the case of direct current flowing through a material such as a resistor one can discuss the effect of low frequency noise.

Other excess low-frequency noise, like burst and popcorn noise, are to be examined in the same low frequency region. This phenomenon is observed in a variety of semiconductor materials.

2.2. THE LOW FREQUENCY NOISE IN CONDUCTORS

Low-frequency noise is manifested in all types of resistors, semiconductor films, thin metal films and vacuum tubes.

The noise power density typically follows the $1/f^n$ characteristics:

$$\overline{v^2(t)} \sim f^{-n} \tag{2.2}$$

where $\overline{v^2(t)}$ is the mean noise power, and n is an experimental constant close to unity. n has been experimentally observed to take on values from 0.8 to 1.3 in various devices [17]. Actually the power spectrum cannot vary as 1/f right down to f = 0, for this would imply an infinite noise power. However, measurements do show a 1/f type spectrum down to frequencies as low as 10^{-4} cycles per second [14].

1/f noise in semiconductor devices is mainly due to the surface defects. The other factors such as generation-recombination of carriers, fluctuation of conductance and distribution of density of states are also of much importance when dealing with sources of low-frequency noise.

Several questions about the low-frequency noise remain unsolved. These important questions may be gathered in three ways [19]. It should be known,

1. Whether the carrier mobility or the carrier number fluctuates,

2. If it is a surface phenomenon or there is a bulk contribution to the noise,

3. If there is a minimum intrinsic noise given by the Hooge relation which states,

$$\frac{S_R(f)}{R^2} = \frac{\alpha_H}{N} \frac{1}{f} \tag{2.3}$$

where $S_R(f)$ is the power spectrum of the resistance fluctuations

N is the number of charge carriers

α_H is a dimensionless constant, 2.10^{-3} .

For a conductor of length L and crossection A, with number of electrons n and mobility μ per unit volume, the conductivity is then written as,

$$\sigma = q \mu n \tag{2.4}$$

and the resistance is,

$$R = \frac{L}{\sigma A} = \frac{L}{q \mu nA} = \frac{L^2}{q \mu N} \tag{2.5}$$

where N is the total number of charge carriers.

From the expression (2.5), it appears that only μ and N may fluctuate. If N fluctuates number-fluctuation noise is considered; if μ fluctuates mobility-fluctuation noise becomes dominant [16]. Likewise, if ΔN and $\Delta\mu$ are statistically independent fluctuations, then,

$$\frac{\Delta R}{R} = - \frac{\Delta N}{N} - \frac{\Delta \mu}{\mu} \tag{2.6}$$

and

$$\frac{S_R(f)}{R^2} = \frac{S_N(f)}{N^2} + \frac{S_\mu(f)}{\mu^2} = \frac{S_V(f)}{V^2} \tag{2.7}$$

where R, N, μ and V are the average values.

Assuming that 1/f noise is due to fluctuations in the mobility of free charge carriers and there is a bulk effect in addition to surface effect, Hooge indicates the following relationship [13]:

$$\frac{\overline{g^2(t)}}{G^2} = \frac{\alpha}{N} \frac{\Delta f}{f} \tag{2.8}$$

where G is conductance

g(t) is conductance fluctuation

α is constant

As most experiments have proven 1/f noise is always present when an electric current is flowing. These experiments are generally restricted to the use of direct exciting current. By the presence of an exciting signal the conduction fluctuation causes current (or voltage) fluctuation, i.e.,

$$\begin{gathered} i(t) = V_{dc}\, g(t) \\ \left[v(t) = I_{dc}\, r(t) \right] \end{gathered} \tag{2.9}$$

2.3. NOISE GENERATION MECHANISM IN AMORPHOUS SILICON

As mentioned previously, in amorphous materials conduction at room temperature is determined by phonon-assisted hopping mechanism. This makes it possible to expect that fluctuations in the phonon assisted hopping rate, p, are responsible for the noise [10].

The probability that an electron jumps from one site to another is given by Equation (1.6). The hopping conductivity is,

$$\sigma = q\mu kTN(E_F) = q^2 DN(E_F) \tag{2.10}$$

where $N(E_F)$ is the density of states per cm^3 per eV near Fermi energy

level, and D is the diffusion constant for electrons:

$$D = \frac{kT}{q} \mu = (1/6) \nu R^2 e^{-2\alpha R} e^{-W/kT} \qquad (2.11)$$

Equation (2.11) can be simplified into the form:

$$D = (1/6) p R^2 \qquad (2.12)$$

Note that R is the hopping distance and p is the phonon assisted hopping rate.

The average conductivity can be rewritten as:

$$\sigma = (1/6)\, q^2\, p\, R^2\, N(E_F) \qquad (2.13)$$

The instantaneous conductivity is,

$$\sigma = (1/6) \frac{q^2 R^2}{kT\Omega} \sum_{i=0}^{kTN(E_F)\Omega} p_i \qquad (2.14)$$

In this equation fluctuations in p are taken into consideration and subscript i refers to the i.th electron with the hopping process. The total number of participating electrons is $kTN(E_F)\Omega$ and the effective sample volume is Ω .

The random fluctuations Δp in the phonon-assisted hopping rate cause random fluctuations $\Delta\sigma$ in the conductivity:

$$\frac{\overline{\Delta\sigma^2}}{\overline{\sigma}^2} \sim \frac{\overline{\Delta p^2}}{\overline{p}^2} \qquad (2.15)$$

Spectral density function for conductivity fluctuations can be determined by applying the Hooge's formula [13],

$$\frac{\overline{\Delta\sigma^2}}{\overline{\sigma}^2} = \frac{\alpha_H}{N.f} \qquad (2.16)$$

Accordingly,

$$\frac{\overline{\Delta\sigma^2}}{\overline{\sigma}^2} = \frac{\alpha_H}{kTN(E_F)\Omega\, f} \qquad (2.17)$$

with the total number of electrons given by $kTN(E_F)\Omega$.

For the d.c. biased a-Si samples, the conductivity fluctuations become voltage or resistance fluctuations with similar spectral density fuction:

$$\frac{S_V}{V^2} = \frac{S_R}{R^2} = \frac{\alpha_H}{kTN(E_F)\Omega f} \qquad (2.18)$$

However, the above expression does not hold for hydrogenated amorphous silicon [10].

2.4. NARROW-BAND NOISE DETECTION

Frequency analysis of any signal, whether deterministic or random, involves the uncertainty principle. In order to determine the frequency f at which the measurement is made, a very narrow bandwidth is required. This is a vital condition especially in low-frequency measurements, although a smaller bandwidth requires a greater measurement time [12].

Noise power spectrum measurement is performed using the set-up illustrated in Figure 2.1. This basic arrangement has a high-gain/low-

noise preamplifier and a selectable gain amplifier at its first stage. Also, a tunable narrow-band filter and a true rms-to-dc converter are included in the equipment chain.

At this stage, it is convenient to mention about some theoretical properties of these building bocks. In the following, the narrow-band filter and true rms-to-dc converter sections will be considered briefly.

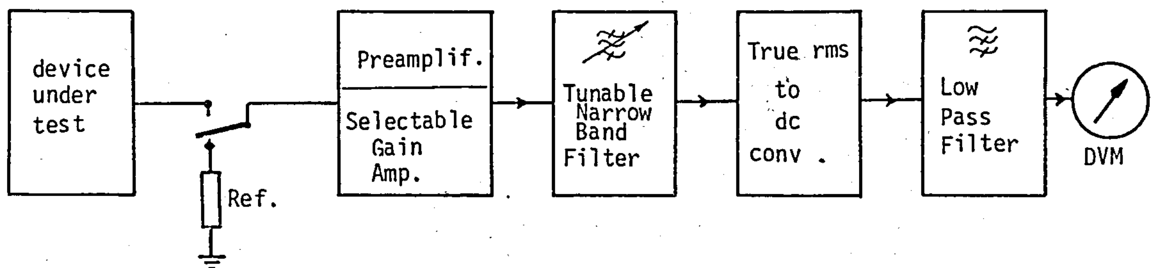

FIGURE 2.1. The schematic of the set-up used for the measurement of noise power spectrum.

2.4.1. NOISE IN A NARROW-BAND FILTER

The ideal band-pass filter has the transfer characteristic given by,

$$|H(f)|^2 = 1 \quad \text{for} \quad (f_c - \frac{f_o}{2}) < f < (f_c + \frac{f_o}{2}) \qquad (2.19)$$

$$= 0 \quad \text{elsewhere}$$

where f_c is the center frequency and f_o is the frequency band.

With the assumption that the power spectrum is constant over the passband f_o and zero elsewhere, while $f_c \gg f_o$, one can notice that,

$$S(f) = S(f_c) \qquad \text{for} \qquad (f_c - \frac{f_o}{2}) < f < (f_c + \frac{f_o}{2})$$
$$= 0 \qquad \text{elsewhere} \qquad (2.20)$$

where S(f) is the power spectrum density of input signal to be processed: (Figure 2.2)

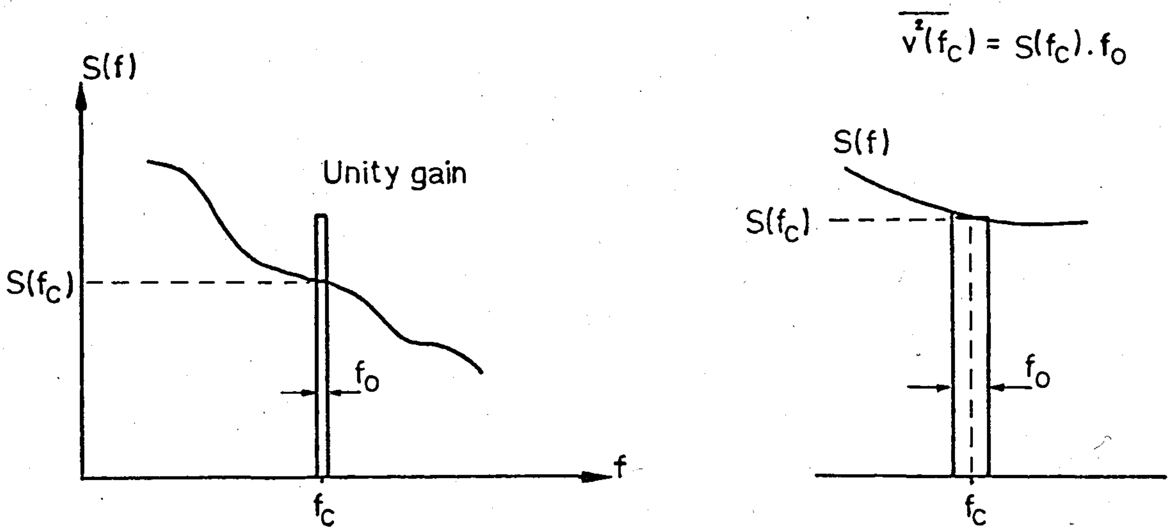

FIGURE 2.2. Power Spectral Density in a norrow band filter

Here S(f) may be assumed to be constant within the the frequency band f_o and equal to $S(f_c)$. The output of the narrow band filter will be more deterministic random signal with the frequency f_c while the input signal is wide band noise: (Figure 2.3)

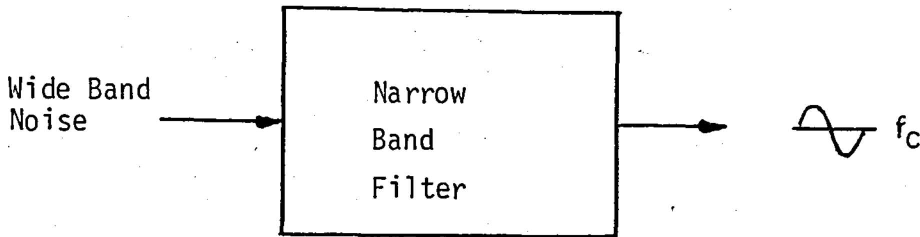

FIGURE 2.3. Input and output of the narrow band filter

This important feature of the narrow-band filter can be specified in terms of autocorrelation function related to narrow-band noise. From Fourier inversion formula, R_V autocorrelation function is,

$$R_V = \int_0^{\infty} S(f) \operatorname{Cos} 2\pi f \tau \, df$$

$$= \int_{f_c - \frac{f_o}{2}}^{f_c + \frac{f_o}{2}} S(f_c) \operatorname{Cos} 2\pi f \tau \, df \qquad (2.21)$$

$$= \frac{S(f_c)}{\pi \tau} \operatorname{Sin}(\pi f_o \tau) \operatorname{COs}(2\pi f_c \tau)$$

Since $f_o \ll f_c$, the noise in a narrow-band filter behaves like a sine wave of midband frequency f_c and its amplitude fluctuates with a frequency approximately equal to $f_o/2$ [12]. That is,

$$v(t) = E(t) \operatorname{Cos}(2\pi f_c t + \emptyset(t)) \qquad (2.22)$$

where both the envelope E(t) and $\emptyset$(t) are slowly varying functions of time.

In the case that no ideal band-pass filters are to be concerned, some form of correction should be taken into account. This correction brings the concept of "effective noise bandwidth". This is not the same as the commonly used 3 dB bandwidth.

The effective noise bandwidth is the bandwidth of the equivalent rectangular filter which will pass the same rms noise as the actual filter:

$$B_n = \frac{1}{|H(f_c)|^2} \int_o^{\infty} |H(f)|^2 df \qquad (2.23)$$

where $|H(f)|$ is the filter transfer function.

2.4.2. TRUE RMS TO DC CONVERSION IN NOISE MEASUREMENTS

When dealing with noise measurements, it is important to take the complex character of the noise signal into account. The calculation of the true rms value of such a signal, negardless of its wave shape, is a desirable feature formany measurement circuits and instruments.

$$v_{rms} = \sqrt{\overline{(v_{in})^2}} \qquad (2.24)$$

where $\overline{(v_{in})^2}$ is the squared mean value of the signal.

The true rms value of a waveform is a more useful quantity than the average rectified value since it relates directly to the power of the signal. The rms value of a statistical signal also relates to its standard deviation.

The direct implementation of equation (2.24) requires three main blocks. The first, a multiplier, will square the input. The second block will be a buffered RC network. The capacitor charges and discharges over each cycle of the input. The net charge, and therefore the voltage across the capacitor, is proportional to the average of the signal from the squarer. The final block will be a multiplier set up as a divider to perform the square root.

Although this technique is direct and apparently simple, it is not very practical. The two multiplier required make the techique expensive. Division (square root) severely limits the amplitude range of the input signal. Errors are difficult or expensive to reduce.

As with many other circuits feedback will help solve the problem. From equation (2.24), squaring both sides gives,

$$v_{rms}^{2} = \overline{(v_{in})^{2}} \quad (2.25)$$

Dividing both sides by v_{rms} (the desired output);

$$v_{rms} = \frac{\overline{(v_{in})^{2}}}{v_{rms}} \quad (2.26)$$

is obtained.

To implement equation (2.26) a three input multifunction IC with the transfer function of

$$v_o = \frac{v_y . v_z}{v_x} \quad (2.27)$$

is used. The integrated circuit yielding the equation above is, like AD433 type IC, a true rms convertor when used with a low cost op-amp

(Figure 2.4). Here,

$$v_z = v_y = v_{in}$$
$$v_x = v_{out} \tag{2.28}$$

and the output of the whole circuit is

$$v_{out} = \frac{\overline{(v_{in})^2}}{v_{out}} \tag{2.29}$$

Comparing this to equation (2.26)

$$v_{out} = v_{rms} \tag{2.30}$$

is written.

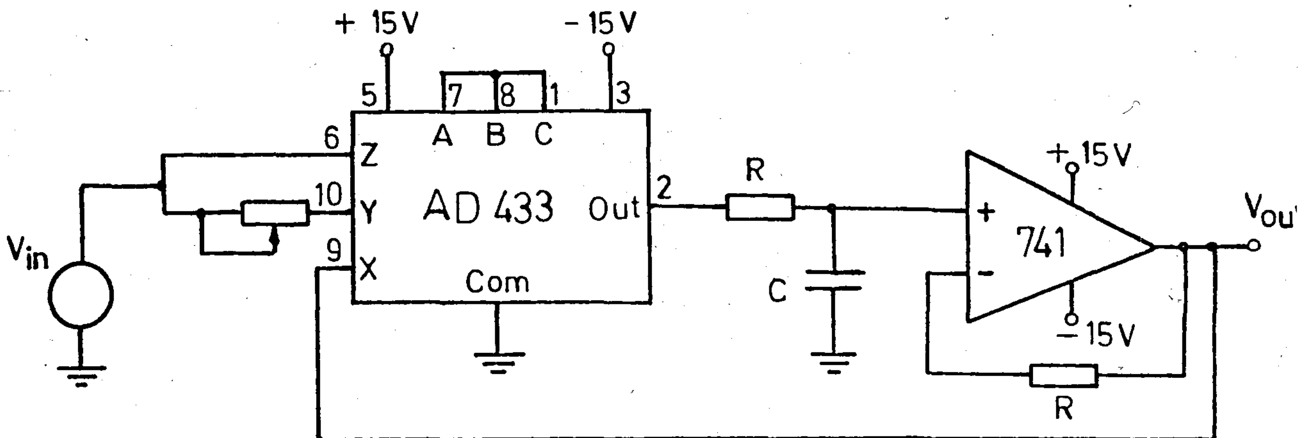

FIGURE 2.4. A True rms Converter proposed for noise measurements

In a like manner true rms to dc conversion helps the measurement of noise signals. Calculation of the true rms value and making this conversion are realized using only one IC chip.

The AD 536 embodies the implicit solution of the rms equation given in (2.26). This solution overcomes the dynamic range as well as other limitations inherent in a straight-forward computation of rms.

The AD 536 is a complete monolithic integrated circuit which performs true rms to dc conversion. It offers performance which is comparable or superior to that of hybrid or modular units costing much more. The AD 536 directly computes the true rms value of any complex input waveform containing ac and dc components. The wide bandwidth of the device extends the measurement capability to 100 KHz which is sufficient in most measurements.

For a Gaussian noise input, using a peak factor of 3, the error involved in direct measurement of rms noise will be about 1%, which is a good approximation for practical purposes. Indeed, the AD 536 has a peak (crest) factor compensation scheme which allows measurements with one per cent error.

The circuitry which is used in noise measurements is shown in Figure (2.5). This is based around an AD 536 chip, which contains all the active circuitry needed to compute the true root-mean-square value of the input waveform [18]. Signals from the filter outputs are selected by a rotary switch and buffered before being fed to the AD 536. The circuit used here has a flat response within ±2% from 0,1 Hz to 60 KHz.

A low-pass filter follows the true rms to dc converter. This second order filter filters out the noise component of the d.c. output, so that, somewhat a steady reading is obtained on the DVM.

BOĞAZİÇİ ÜNİVERSİTESİ KÜTÜPHANESİ

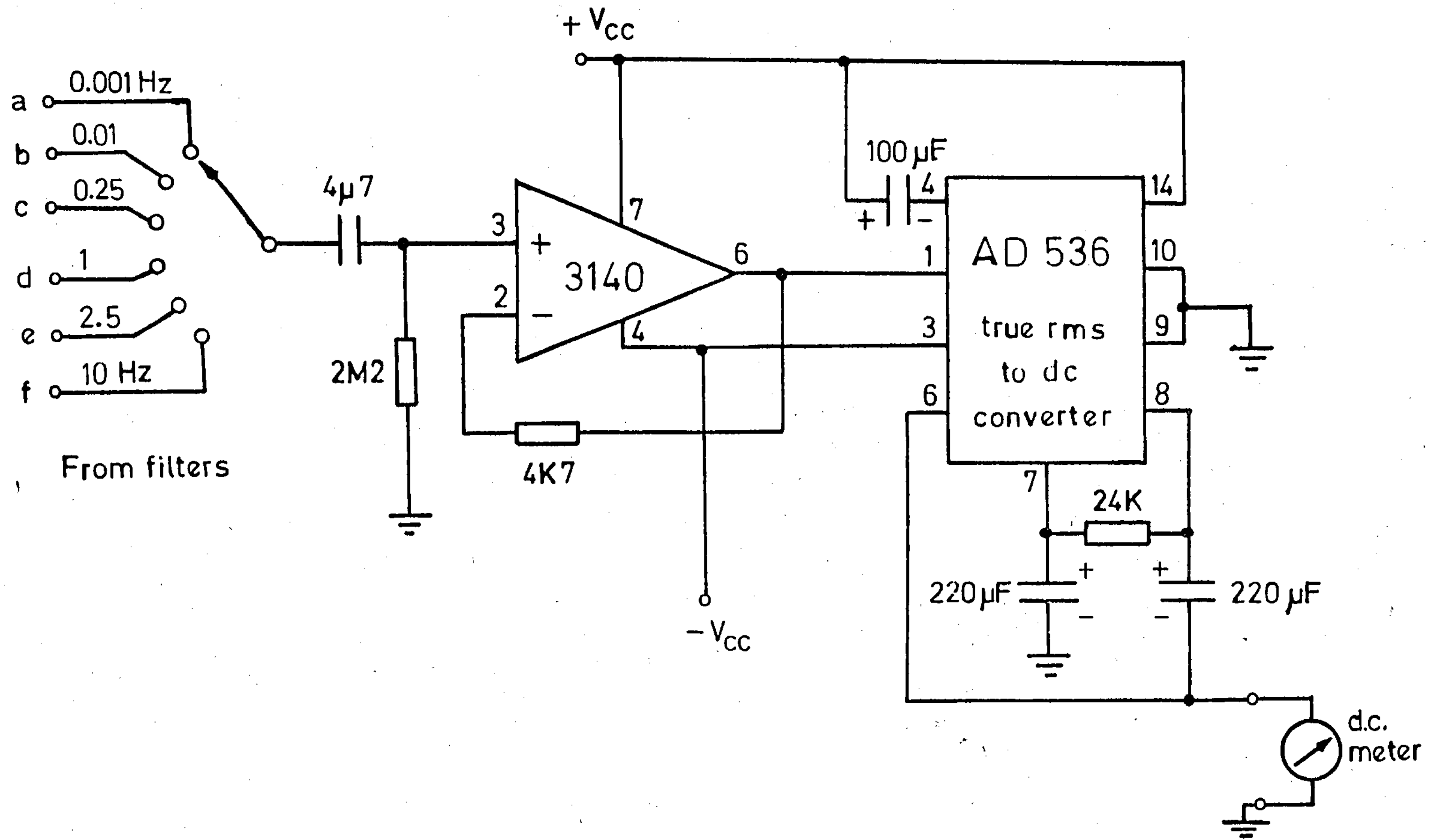

FIGURE 2.5. True rms to dc converter

The waiting time, that is the time period between two consecutive readings, is approximately 2RC. The second order low-pass filter is realized by means of the buffer output of the true-rms-to-dc converter. Internally available op amp and external passive components determine the transfer characteristics of this Butterworth filter:

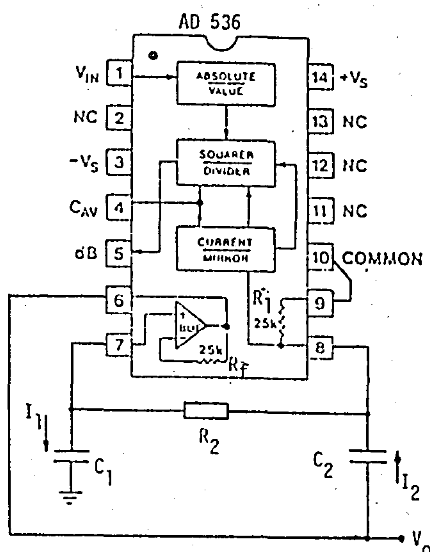

This circuit produces a roll-off of -40 dB/decade. The op amp is connected for d.c. unity gain and resistor R_f is included for d.c. offset. Since the op amp circuit is basically a voltage follower (unity gain ampfier) the voltage across C_1 is equal to output voltage V_o. Therefore,

$$I_2 = - s\ C_2\ R_2\ I_1 \tag{2.31}$$

and the transfer function is:

$$\frac{V_o}{V_{in}} = \frac{(1/\ sC_1)\ I_1}{R_1 I_1 + sC_2 R_1 R_2 I_1 + R_2 I_1 + (1/sC_1)\ I_1} \tag{2.32}$$

If $R_1 \simeq R_2 = R$ and $C_1 \simeq C_2 = C$,

$$\frac{V_o}{V_{in}} = \frac{1}{(\ 1 + sRC\ )^2} \tag{2.33}$$

CHAPTER III

EXPERIMENTAL TECHNIQUES

3.1. PREPARATION OF THE SAMPLES

The preparation of the amorphous silicon films is realized using the vacuum evaporation technique. There are two kinds of structures used in this work. While one type depends on the coplanar geometry, the other one is produced as the sandwich type sample.

The amorphous silicon films and metal electrodes are evaporated on 2.5 x 4.5 cm microscope slides produced by Fischer Scientific Coop. The evaporation masks are made of aluminum metal plates of 0.55 mm thickness.

In order to produce a coplanar geometry, 1.5 x 2.5 cm metal electrode masks are used. Wires of various diameters, such as 0.22 mm, 0.30 mm and 0.37 mm, are placed on the surface of the electrode masks. The smaller the value of diameter, the lower is the sample resistance. The masks used in the preparation of films are shown in Figure 3.1.

Sandwich type samples are also fabricated, such that the amorphous silicon film is settled between two aluminum layers. Aluminum

electrodes used in this process have the dimensions of 1.5 cm x 1 mm. The structure of this type samples are depicted in Figure 3.2

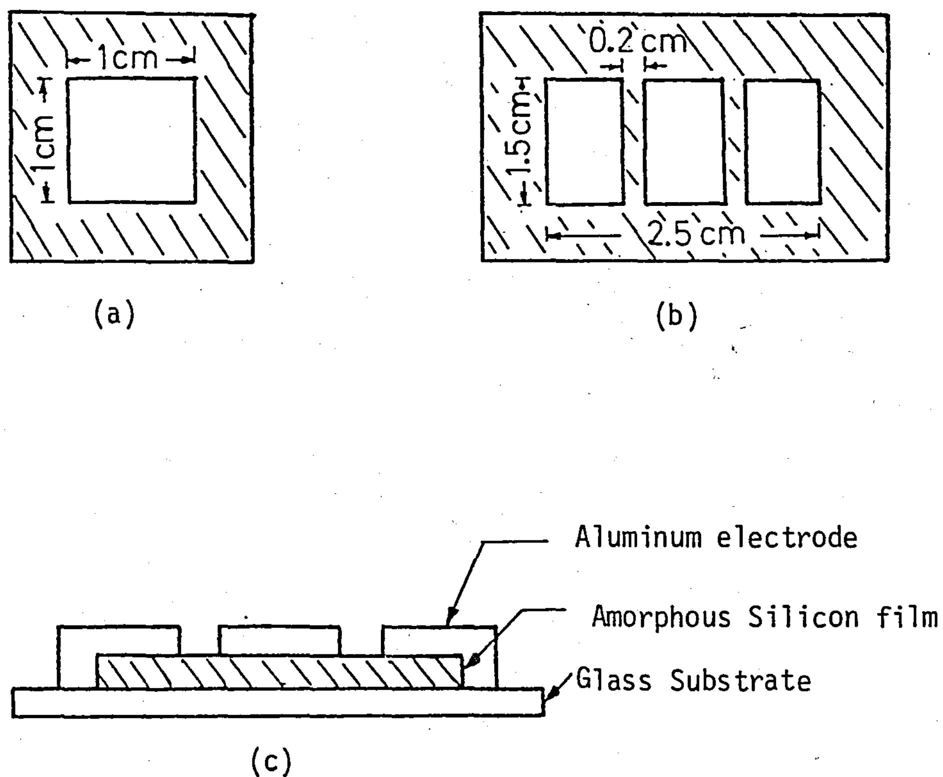

(a) Silicon Mask

(b) Electrode Mask

(c) Cross-section of the prepared film in Coplanar Geometry

FIGURE 3.1. Masks used in the preparation of Coplanar Geometry Samples

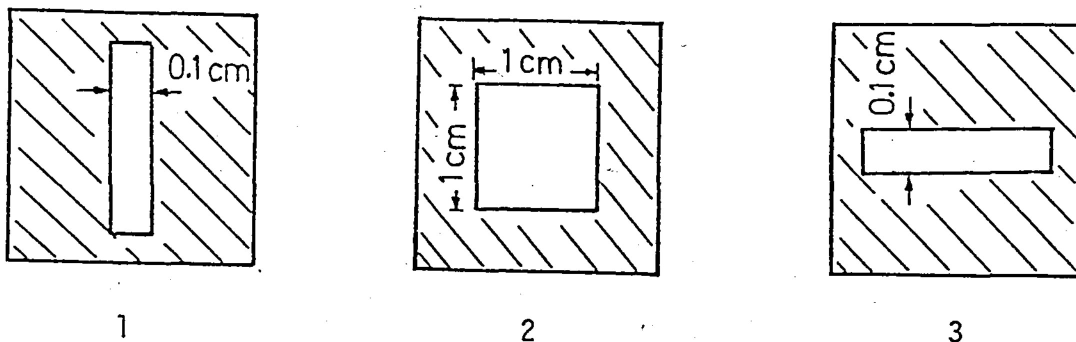

(a)

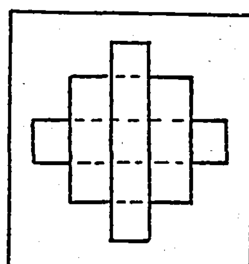

(b)

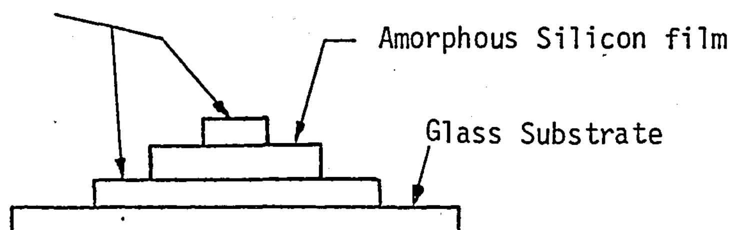

(c)

(a) Masks: 1 and 3 are elctrode masks, 2 is silicon mask

(b) Top View of the prepared film

(c) Cross-section of the prepared film in Sandwich Geometry

FIGURE 3.2. The Preparation of Sandwich Type Films

The manufacturing process for both types is given briefly in the following:

Microscope slides are first cut to the desired dimensions and then cleaned in an ultrosonic cleaner.

The vacuum system used in the preparation is VARIAN VT-422 type. The system is pumped down to 10^{-3} torr pressure with a cryopump. In order to achieve a lower pressure ion pumps are used. The pumping time of the cryopump is nearly one hour. Ion pumps operate continuosly for 24 hours, to reduce the base pressure down to 10^{-7} - 10^{-8} torr. The glass substrates are placed on a substrate holder on which three different masks can be placed simultaneously. This means that three different samples can be produced at a time.

The evaporation system is composed of an electron gun and three crucibles. Evaporant is a pure polycrystal hump. The distance between the evaporant and glass substrate is 25 cm. This distance should be so large that most of the atoms arrive at the substrate along a perpendicular path, otherwise the surface of the film may not be smooth. On the other hand, in order to protect the films from the impurity atom formation, the base pressure must be kept as low as possible.

For the coplanor geometry, the silicon films are grown on the substrate with the thicknesses between 0,30 µm and 0.60 µm. The evaporation of the silicon films takes two to four hours. After the deposition of films, the vacuum system is allowed to cool in order to prevent the formation of an oxide layer on the film. Then the system is opened and prepared for the evaporation of aluminum electrodes. The evaporation of electrodes takes 5 to 10 minutes and the thickness of them becomes approximately 1 µm.

The structure of Figure 3.2 requires three different stages of evaporation. First a thin film of aluminum is grown on the substrate to form the back contact. Then the silicon film is depositioned and finally another aluminum contact is produced as a third layer.

3.2. MEASURING EQUIPMENT

The basic block diagram of the measuring system used is given in Figure 2.1. The first three main blocks consisting of preamplifier, selectable gain amplifier and tunable narrow band filter were supplied as one instrument called Heterodyning Lock-In Amplifier. This Lock-In amplifier is ITHACO, Dynatrac 391A type.

The front-end facilities of the Lock-In amplifier make this instrument usable in noise measurements or similar experiments. This amplifier is to be used as a variable frequency (0-4.4 kHz), variable bandwidth (0.0001-100 Hz) noisemeter with its variable gain (sensitivity max. 120 dB) A broadband front-end with its flat frequency and phase response can handle an input signal whose frequency drifts or changes without producing a corresponding phase drift or change between its input and output signals.

The Lock-In amplifier provides a front-end variable band filter which automatically tracks changes in the frequency of the signal to be measured; this tracking filter action eliminates the manual retuning. It also provides exceptional performance in such critical areas as overload capability, output stability, sensitivity and self noise.

The input signal is amplified by the preamplifier and the variable gain signal amplifier. The very low self noise of the instrument is determined by the preamplifier. A 24 dB/octave low-pass filter after the amplifier attenuates unwanted frequencies above the frequency range in use.

The output of the Lock-In amplifier is connected to the input of the true rms to dc converter. This converter circuit is given in Figure 2.5. And finally the readings are taken from a conventional DVM used as a dc meter.

The selectable frequency range of the Lock-In amplifier is from several Hz upto 1.1 kHz. Above this frequency an external referance signal generator whose frequency can be varied upto 4,4 kHz is connected via the frequency-out of the instrument. The frequency-out socket is also important to determine the operating frequency precisely using a frequency counter.

Especially in low frequencies below 150-200 Hz, the bandwidth of the filter should be kept small in order to prevent the effect of 50 Hz. mains frequency. Furthermore the measuring frequencies are accordingly chosen far from the harmonics of 50 Hz, like 175 Hz, 225 Hz etc., to ged rid of the interfering spurious effects.

The other major difficulty encountered with the noise measurement is the environmental noise. For this reason every connection has to be shielded type. By the same reason explained above, the samples are hold in a shielded sample holder.

3.3. 1/f NOISE WITH D.C. EXCITATION

3.3.1. Theoretical Considerations

It is only possible to observe the 1/f noise when an excitation current is present. The circuit arrangement of Figure 3.3 is used to d.c. bias a pair of amorphous silicon films, of equal resistances [11]. The bridge circuit output is then given by,

$$v_o(t) = V_s - \frac{2V_s R_1(t)}{R_1(t)+R_2(t)} \tag{3.1}$$

where $R_1(t) = R_1 + r_1(t)$ and $R_2(t) = R_2 + r_2(t)$ are sample resistances, with resistance fluctuations $r_1(t)$ and $r_2(t)$.

Assuming that $R_1 \simeq R_2 = R$ and $r(t) \ll R$, Equation (3.1) can be rewritten as,

$$v_o(t) = \frac{V_s}{2} \left[\frac{r_2(t)}{R} - \frac{r_1(t)}{R} \right] \tag{3.2}$$

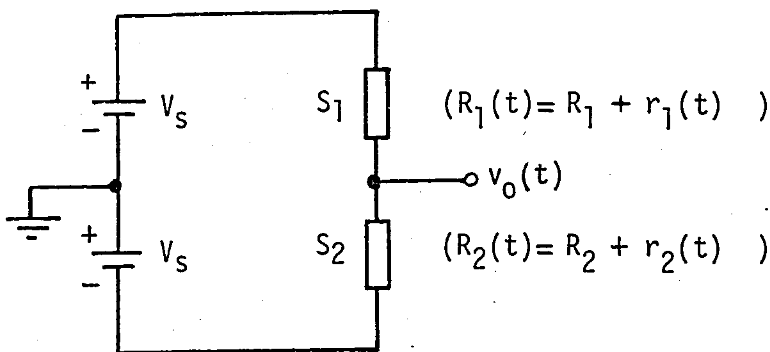

FIGURE 3.3. D.C. Biasing of the amorphous silicon samples

The bridge output will contain no d.c. component due to the bridge symmetry.

The uncorrelated random fluctuations $r_1(t)$ and $r_2(t)$ give rise to the mean square voltage fluctuations;

$$\overline{v_o^2(t)} = \frac{v_s^2}{4}\left[\frac{\overline{r_1^2(t)}}{R^2} + \frac{\overline{r_2^2(t)}}{R^2}\right] \qquad (3.3)$$

Taking,

$$\overline{r_1^2(t)} \simeq \overline{r_2^2(t)} = \overline{r^2(t)},$$

$$\overline{v_o^2(t)} = \frac{v_s^2}{2}\left[\frac{\overline{r^2(t)}}{R^2}\right] \qquad (3.4)$$

and substituting Equation (2.18) for $\overline{r^2(t)}/R$,

$$\overline{v_o^2(t)} = \frac{v_s^2}{2} \frac{\alpha_H}{kT\Omega N(E_F)f} \qquad (3.5)$$

Sandwhich type samples, however, show capacitive properties due to their geometry. The sample capacitance effectively attenuates the output noise voltage and this effect is more pronounced at high frequencies with the sample capacitances taken into account. The output voltage is then (Figure 3.4),

$$v_{n_o} = (v_1 + v_2)\frac{R // \frac{1}{2sC}}{R + (R // \frac{1}{2sC})} \qquad (3.6)$$

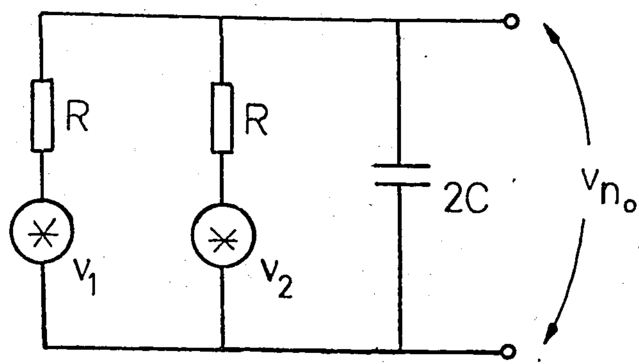

FIGURE 3.4. Equivalent noise circuit with sandwich type samples

Supposing that,

$$\overline{v_1^2} \simeq \overline{v_2^2} = \overline{v^2} \tag{3.7}$$

and assuming uncorrelated noise voltages,

$$(\overline{v_{n_o}^2})^{1/2} = (\overline{v^2})^{1/2}\sqrt{2}\ \frac{1}{2RCs + 2} \tag{3.8}$$

Resulting in a correction factor of,

$$\text{C.f.} = \sqrt{4 + (4\pi fRC)^2} \tag{3.9}$$

Expression (3.9) is used to correct for the capacitive effects in noise measurements.

Normally, noise measurements are specified in mean noise power, namely $volt^2$ per unit bandwidth. Instead, the concept of effective noise resistance, R_n, is introduced as a more convenient way of expressing the results on noise measurements. The results so obtained are normalized with respect to thermal noise from a low-noise type resistor. Parameters, such as the effective noise bandwidth, the measuring system gain and the ambient temperature are therefore eliminated.

On the other hand, the Lock-In amplifier used in measurements can be represented with its current and voltage noise sources, and a noise-free amplifier. (Figure 3.5) If the input of the amplifier is short-circuited (R = 0), the output gives the value of $(\overline{e_n^2})^{1/2}$. Moreover, when the input is open circuit, or $R \gg R_{in}$,the noise voltage from amplifier determines the order of the magnitude of the noise current source i_n.

$$\overline{v_{n_o}^2}\ (s.c.) = \overline{e_n^2}\ A_v^2$$

$$\overline{v_{n_o}^2}\ (o.c.) = \overline{i_n^2}\ R_{in}^2\ A_v^2$$

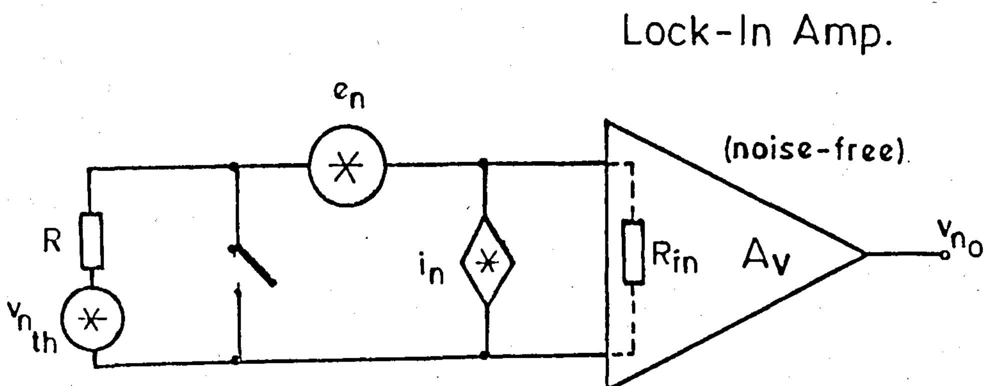

FIGURE 3.5. Equivalent representation of the amplifier by its noise sources with noise-free amplifier

3.2.2. Summary of Experimental Results

The following experiments are carried out in order to gain a better insight to the generation of low-frequency noise in amorphous silicon films.

The measurement results are corrected for the residual system noise wherever it is found to be necessary. However, in most experiments, system noise is negligibly small. The short-circuit input noise characteristics for the Lock-In amplifier is given in Figure 3.6.

The readings are taken at 2RC time intervals in order to obtain statistically independent results.

Before attempting to any noise measurement, the samples are checked for ohmic contacts by applying a d.c. bias. The typical I-V curve of an amorphous silicon sample is given in Figure 3.7. It can be seen that the samples possess ohmic behaviour for d.c. voltages 0-20 Volts, over the region of noise measurements.

For the sandwich type samples, the capacitive effect is investigated for the frequency range of interest and plotted in Figure 3.8. Capacitance versus frequency graph further used for correction in noise measurements of sandwich amorphous silicon samples.

When plotted as a function of frequency, the low-frequency noise from the sandwich films obeys the $1/f^n$ law, with index n taking values of 1.1 to 1.25. In Figure 3.9 and 3.10, two such measurements are illustrated for samples from the same batch for comparison.

Amorphous silicon films produced in coplanar geometry show similar low-frequency characteristics as shown in Figure 3.11, 3.12 and 3.13 .

Index n is found to vary between 1.2 and 1.35 for these samples.

Noise power measurements at different d.c. excitation levels are in good agreement with the Equation (3.5). Figure 3.14 and 3.15 show the effective noise resistance (power) for increasing d.c. excitation for samples in coplanar and sandwich type geometry respectively.

1/f noise in crystalline silicon films is also considered for comparison with the amorphous samples using the same measuring equipment (Figure 3.16).

The data obtained at 800 Hz for the crystalline and amorphous silicon samples respectively are given below:

Amorphous Silicon	Crystalline Silicon
$R_{d.c.} \cong 30\ M\Omega$	$R_{d.c.} \cong 4\ K\Omega$
$V_{d.c.} = 5\ V$	$V_{d.c.} = 1\ V$
$I_{d.c.} = 5/30 \times 10^6\ A$	$I_{d.c.} = 1/4 \times 10^3\ A$
$R_n = 0.38\ M\Omega$	$R_n = 0.58\ G\Omega$

Since noise power is directly proportional to $I^2_{d.c.}$; under the same conditions, the d.c. current through the crystalline sample would be larger, therefore it is necessary to normalize the noise measurements with respect to $I^2_{d.c.}$:

For amorphous silicon : $1.36 \times 10^{19}\ \Omega/A^2$

For crystalline silion : $9.28 \times 10^{15}\ \Omega/A^2$

From the above it is obvious that amorphous silicon samples are much noisier than crystalline ones, with the mean noise power ratios of 10^3 to 1.

A further measurement is done to investigate the temperature dependence of the low-frequency noise in amorphous silicon. The sample temperature is varied from 300^oK upto 440^oK. The $1/f^n$ type spectrum is shown to be valid at all temperatures, however decreases with increasing temperature (Figure 3.17). As a further observation n is measured to increase to a value of 1.45 at 440^oK.

Typical $R_n - V_{dc}^2$ characteristics for a coplanar sample at 400^oK is shown in Figure 3.18. The temperature dependence measurements are realized with the samples stored in a thermostatic chamber. The ambient temperature is electronically controlled.

Finally, using the Equation (3.5) and taking the calculated $N(E_F)$ values which are determined from d.c. conductivity measurements on similar samples, Hooge's empirical constant is to be obtained for a-Si samples.

For a sadwich type sample (volume $\Omega = 6.10^{-7}$ cm^3 and at room temperature $KT = 0.025$ eV) with $N(E_F)$ is in the order of 10^{19}, it is determined that $\alpha_H = 33.10^{-3} = 3.3.10^{-2}$. This value is in the accepted range given by Hooge [13].

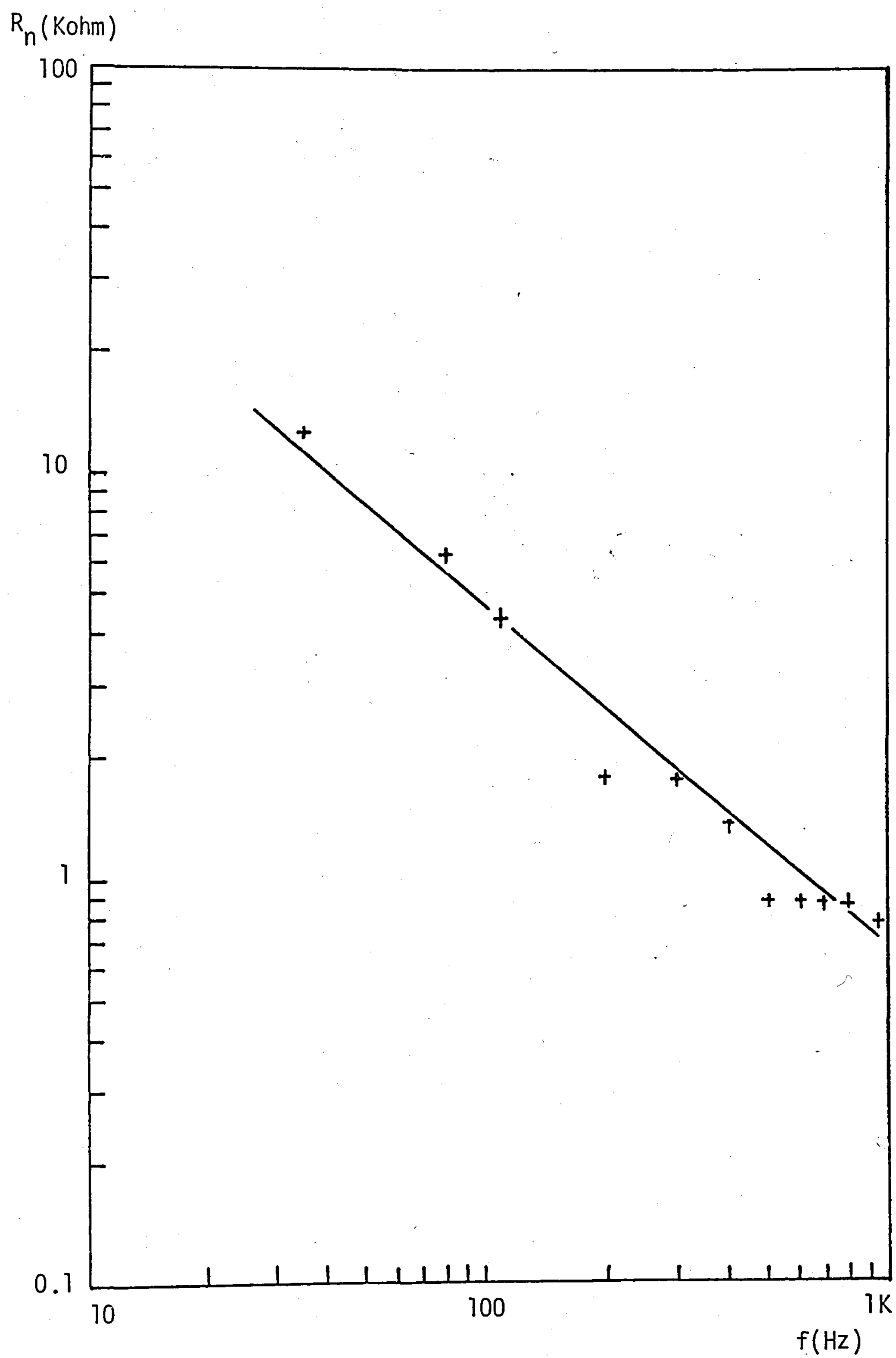

FIGURE 3.6. System Noise Characteristics

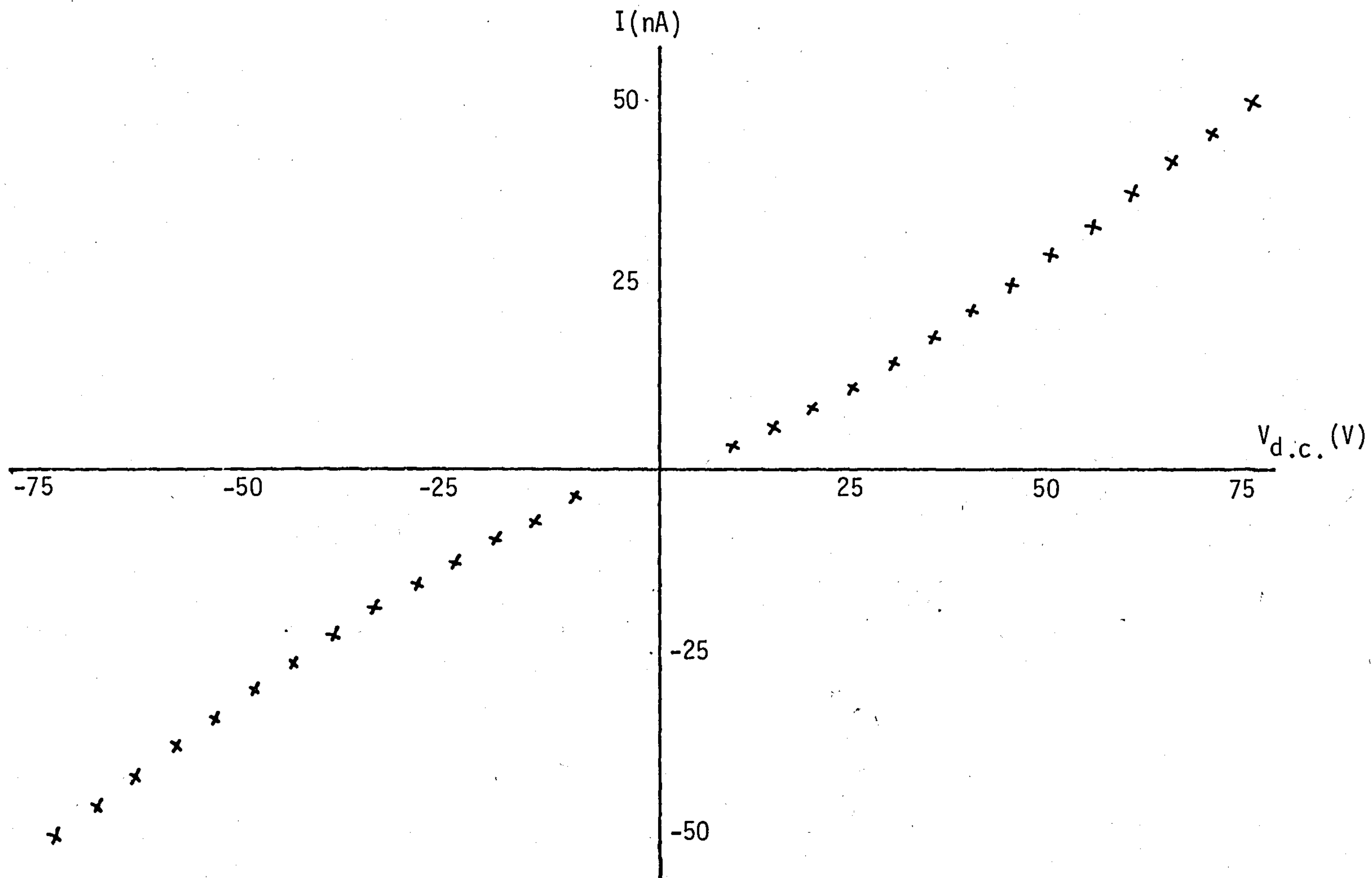

FIGURE 3.7. Typical I-V Curve of a Sample at Room Temperature

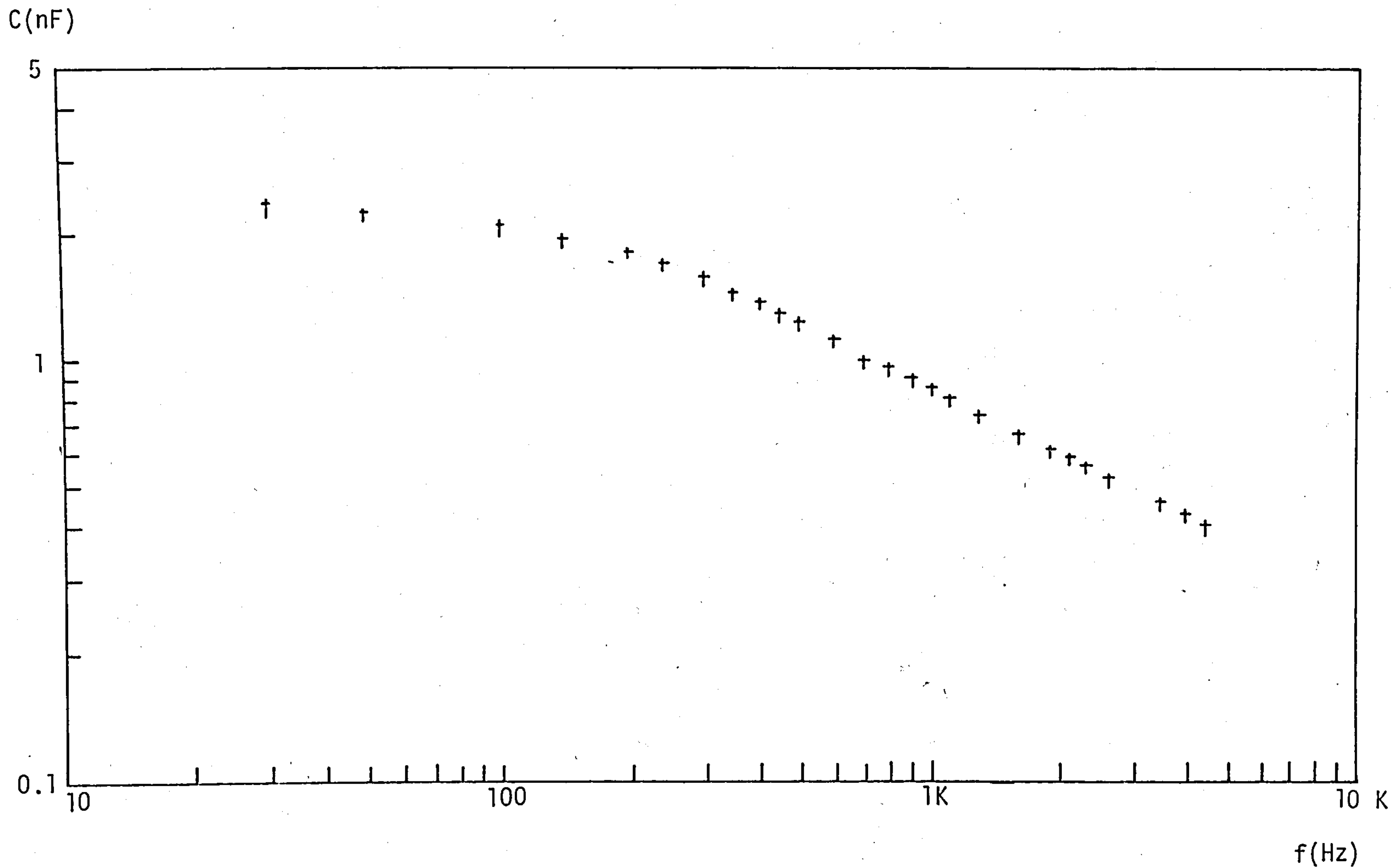

FIGURE 3.8. Typical C versus f Graph of a Sandwich Type Sample

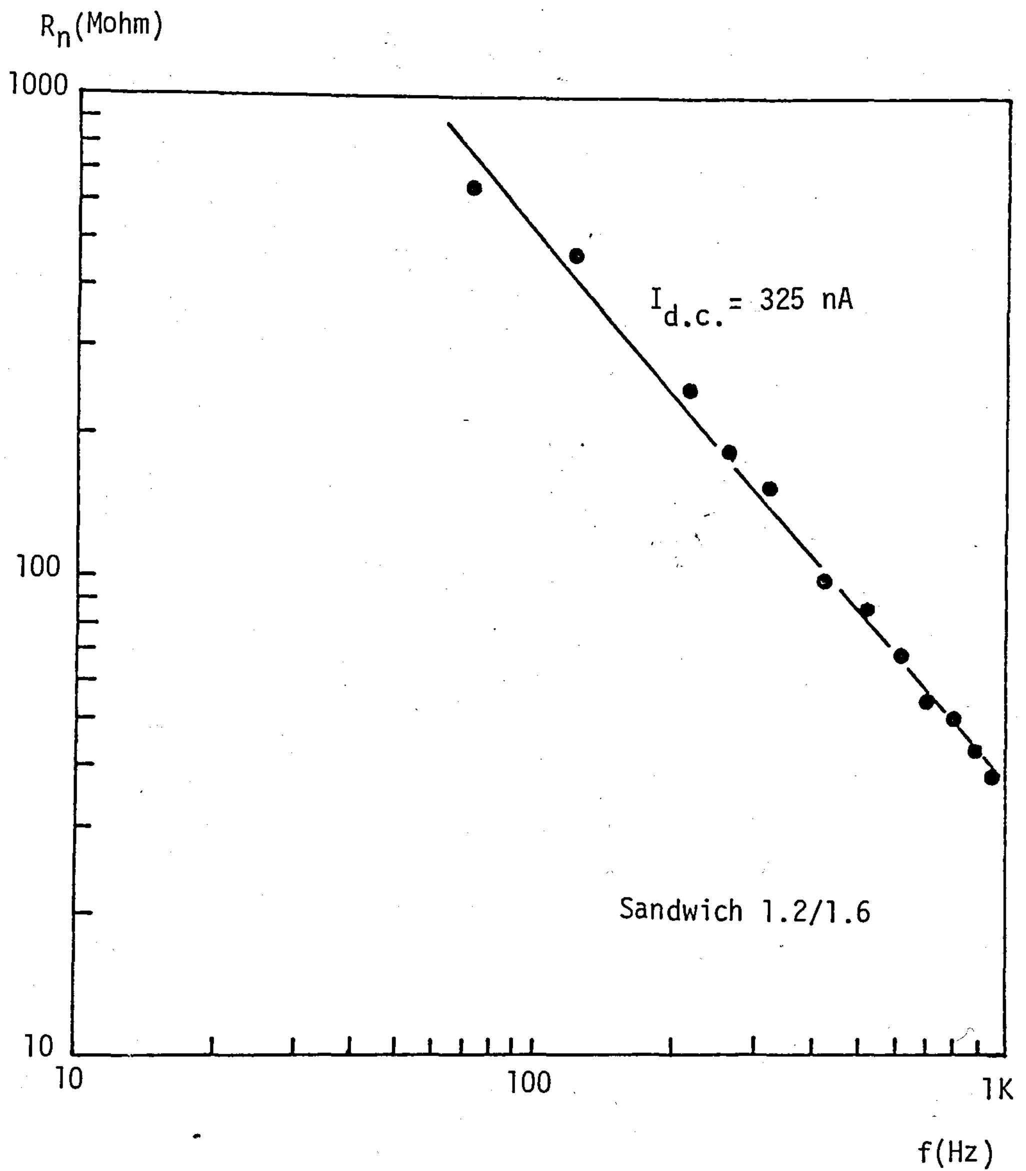

FIGURE 3.9. Low-Frequency Noise of the Sandwich Sample no.1

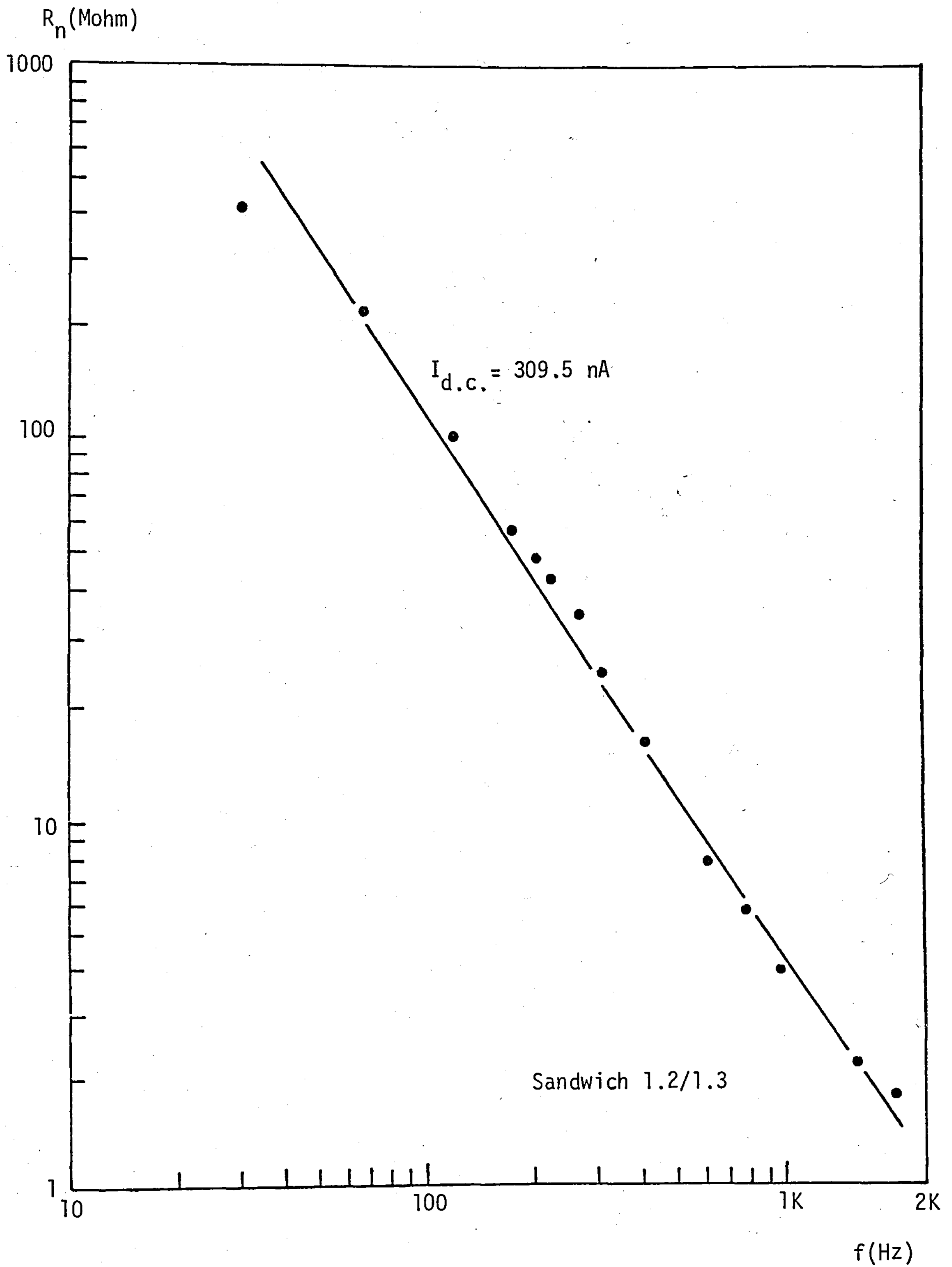

FIGURE 3.10. Low-Frequency Noise of the Sandwich Sample no.2

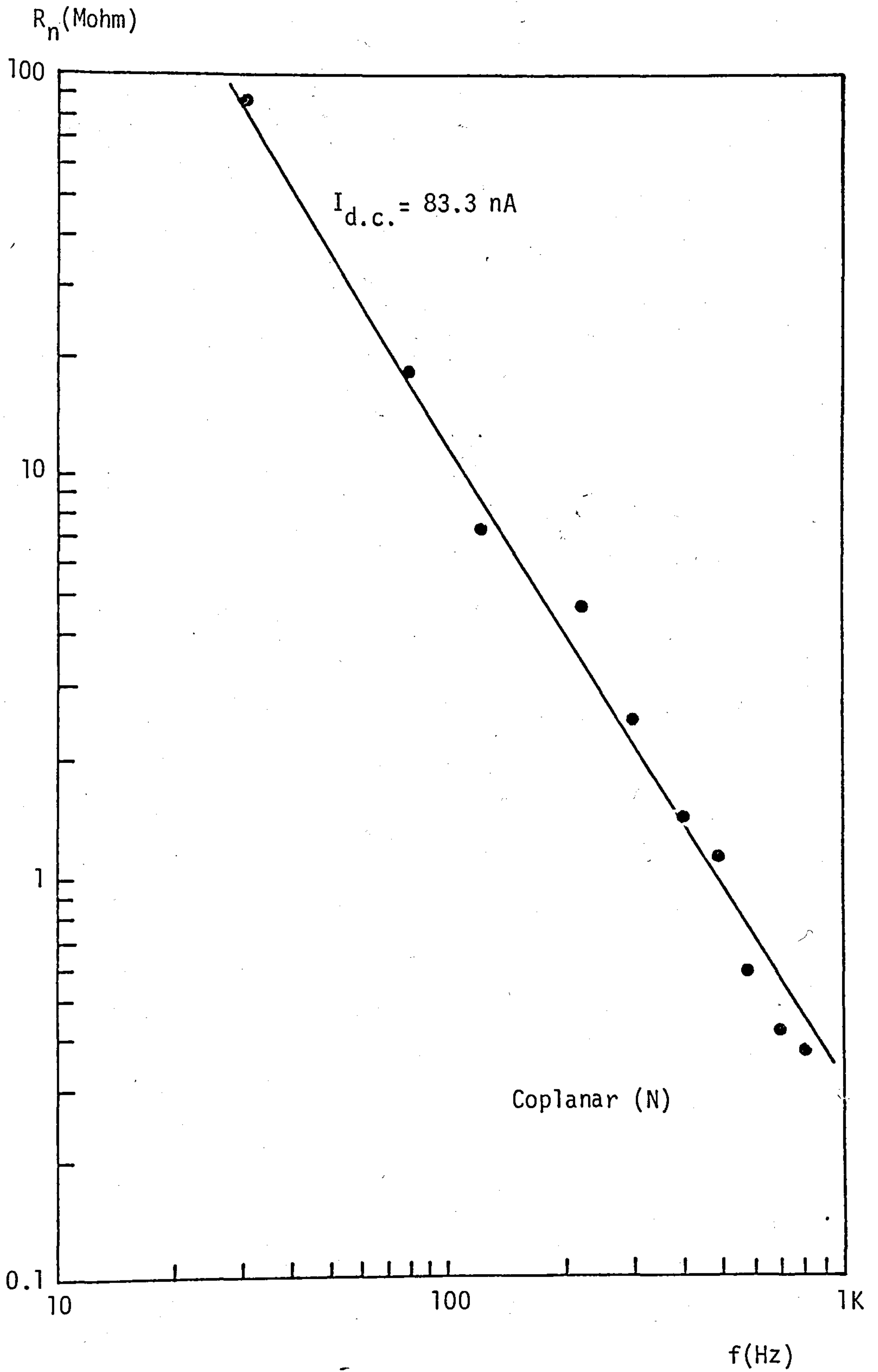

FIGURE 3.11. Low-Frequency Noise of the Coplanar Sample no.1

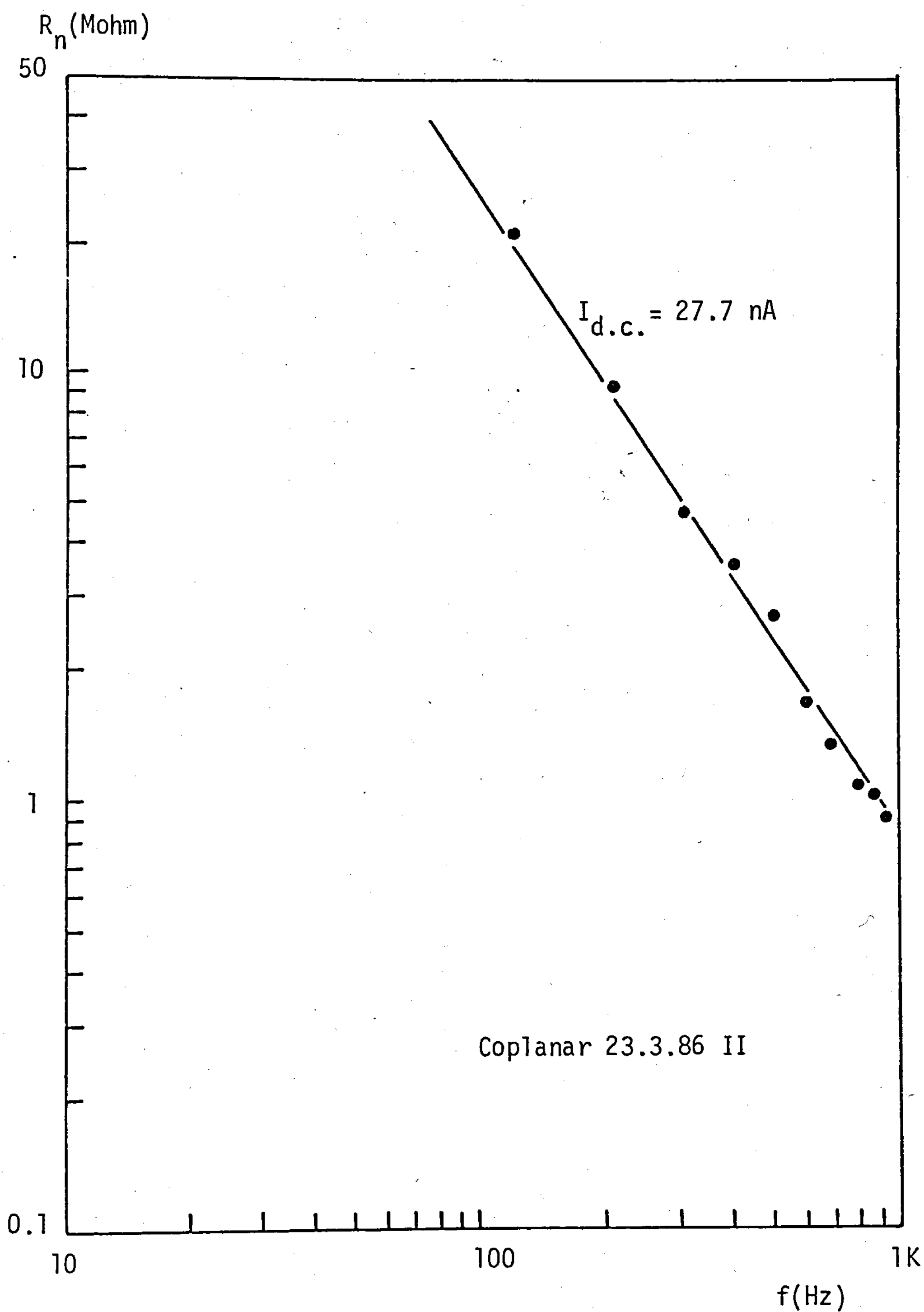

FIGURE 3.12. Low-Frequency Noise of the Coplanar Sample no.2

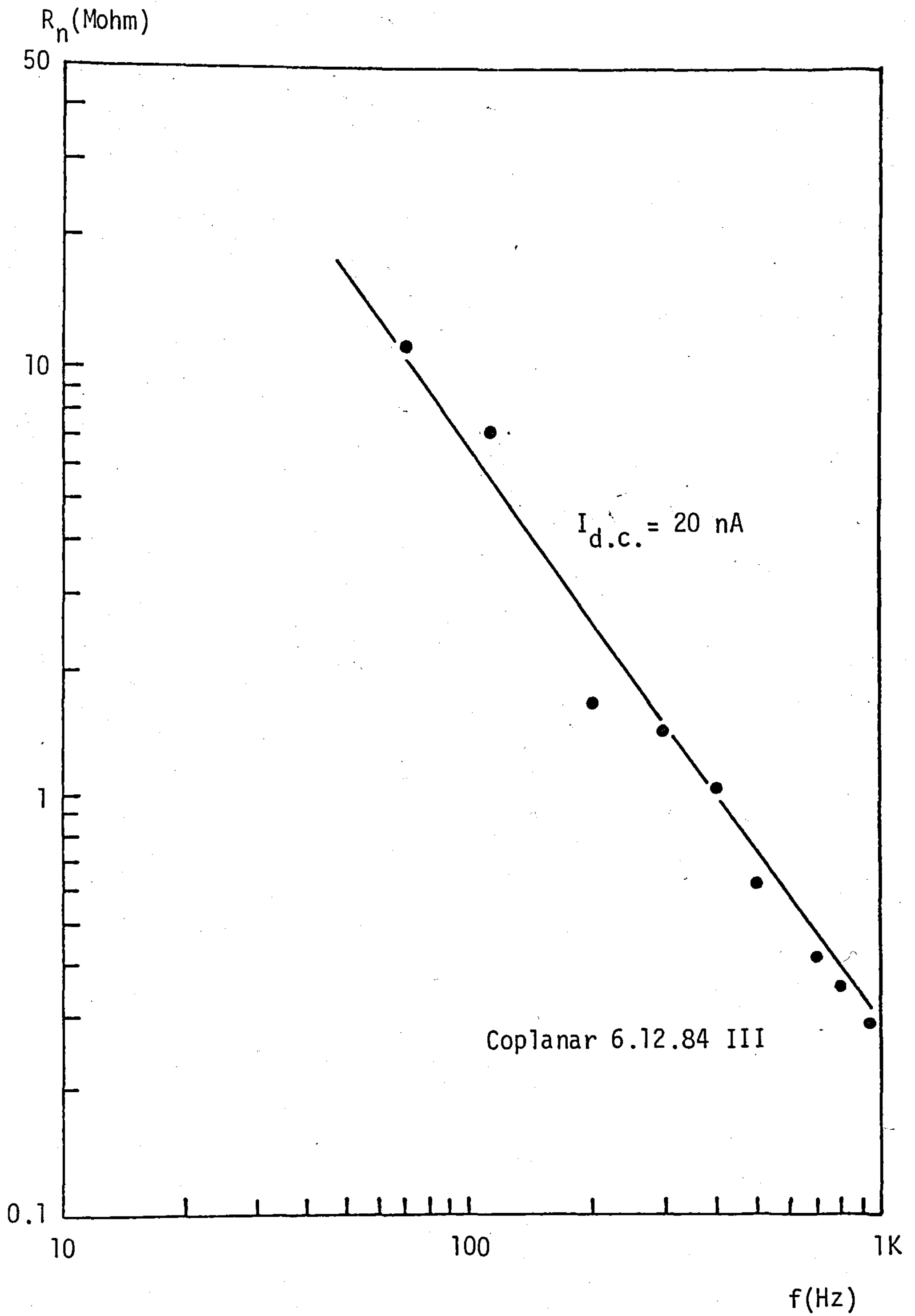

FIGURE 3.13. Low-Frequency Noise of the Coplanar Sample no.3

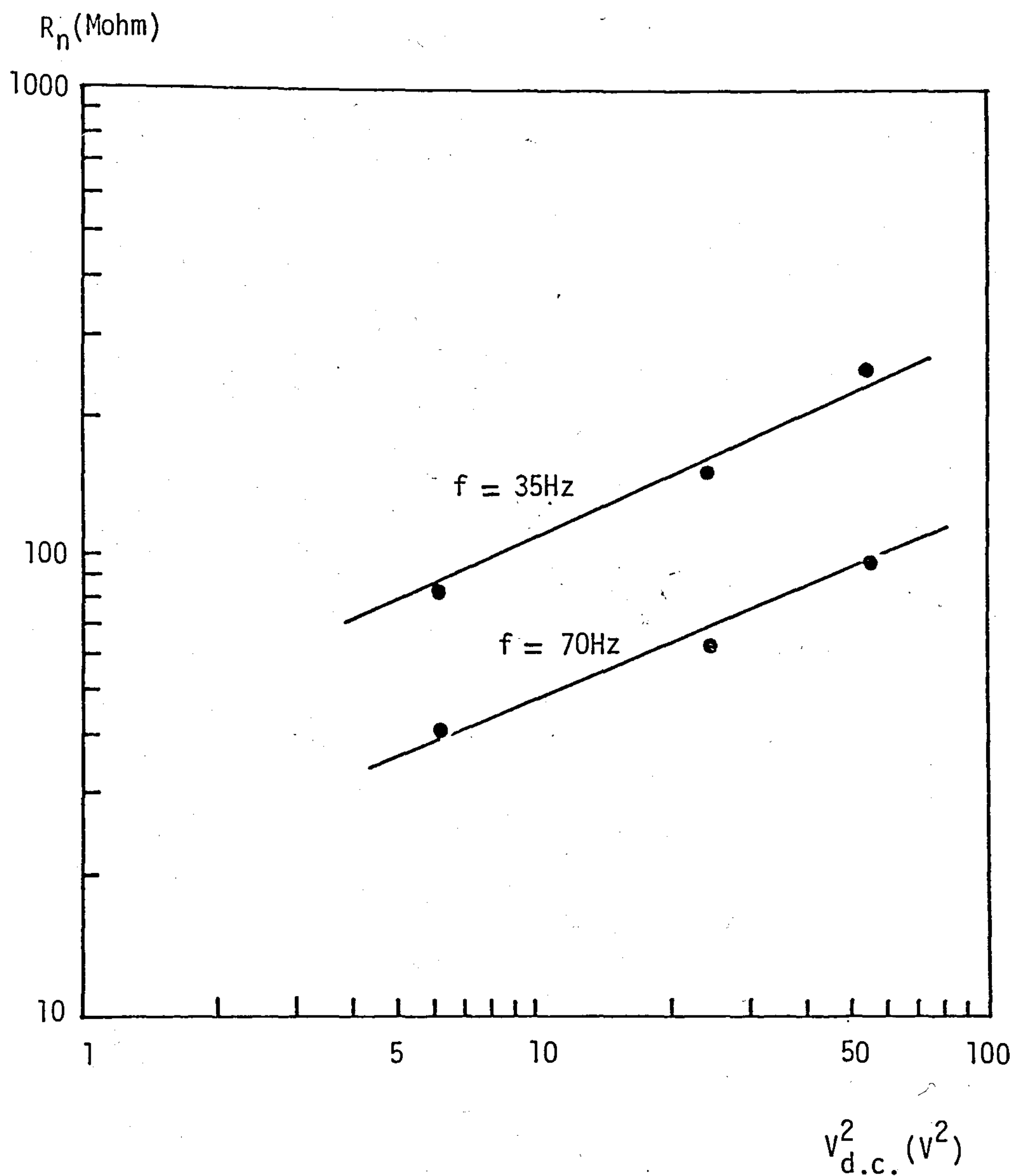

FIGURE 3.14. Effective Noise Resistance versus $V_{d.c.}^2$ Graph of a Coplanar Sample

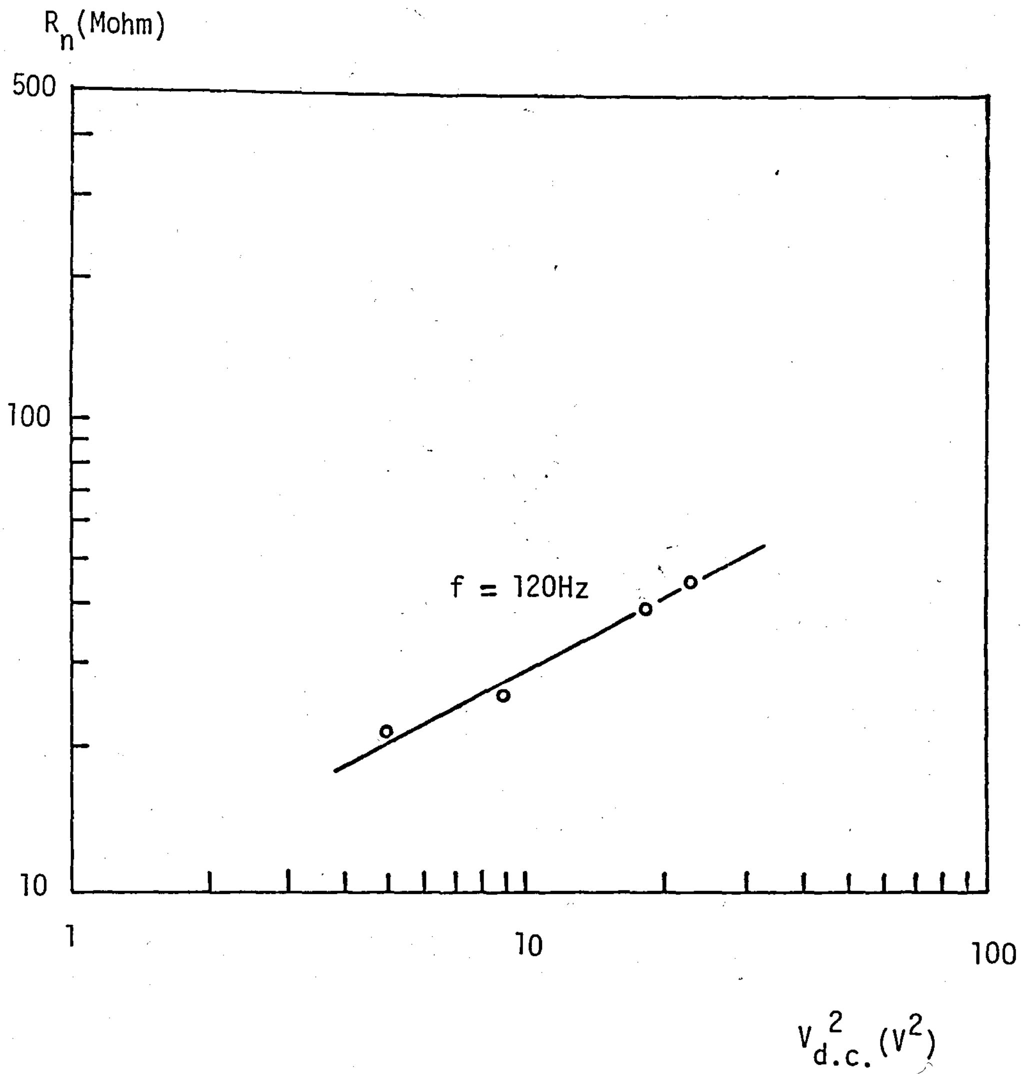

FIGURE 3.15. Effective Noise Resistance versus $V_{d.c.}^2$ Graph of a Sandwich sample

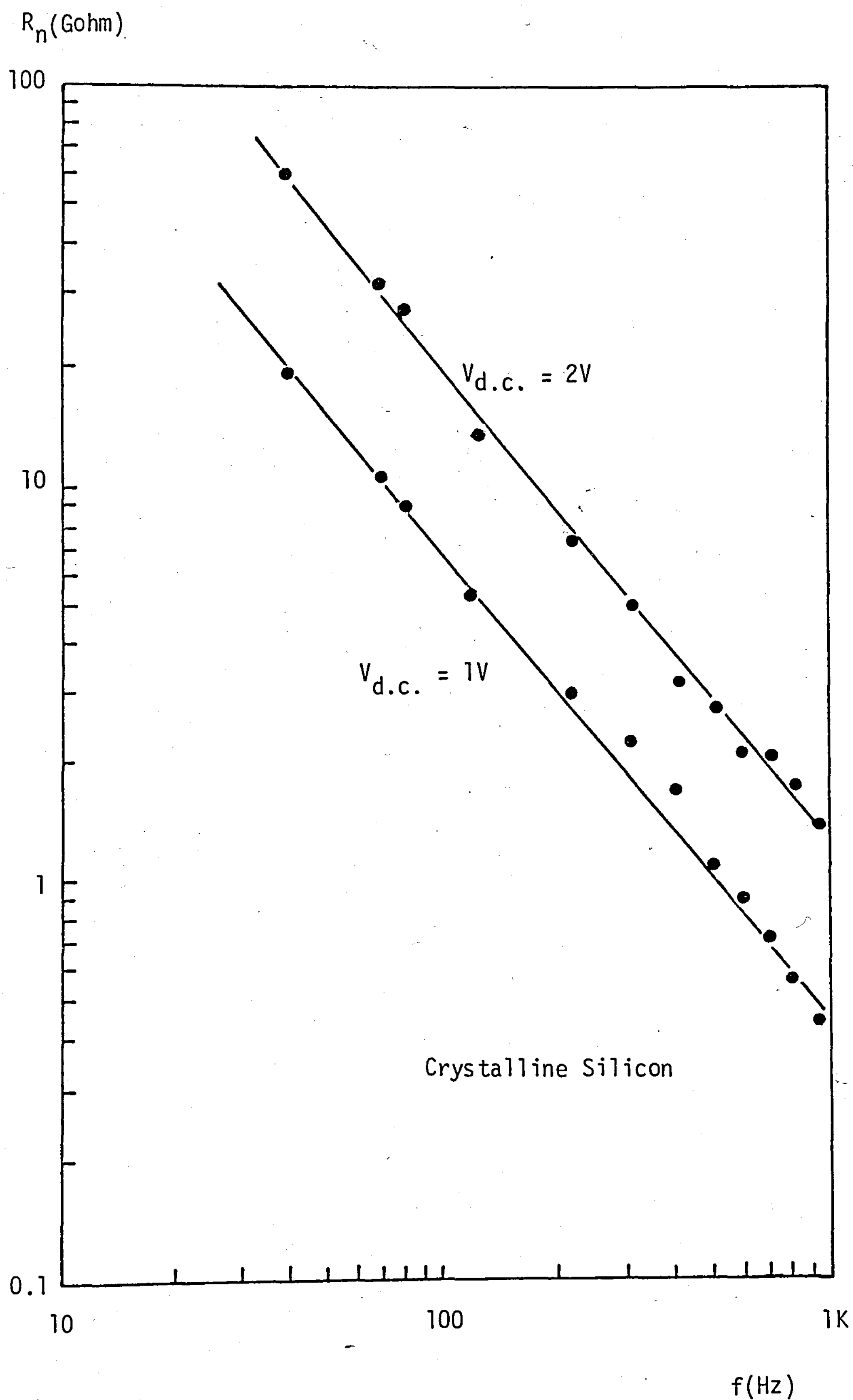

FIGURE 3.16 1/f Noise in a Crystalline Silicon Film

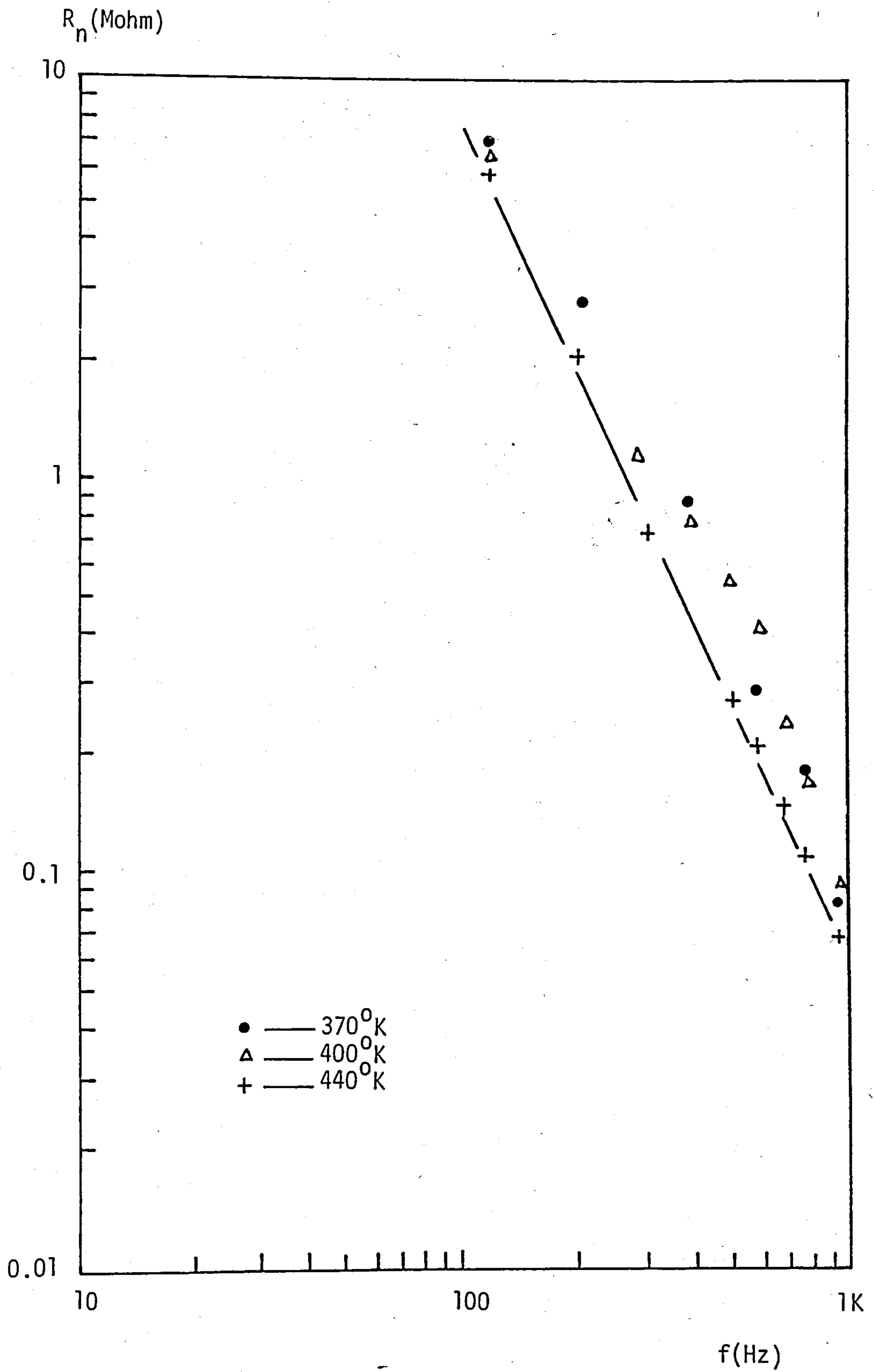

FIGURE 3.17 Temperature Depencence of 1/f Noise

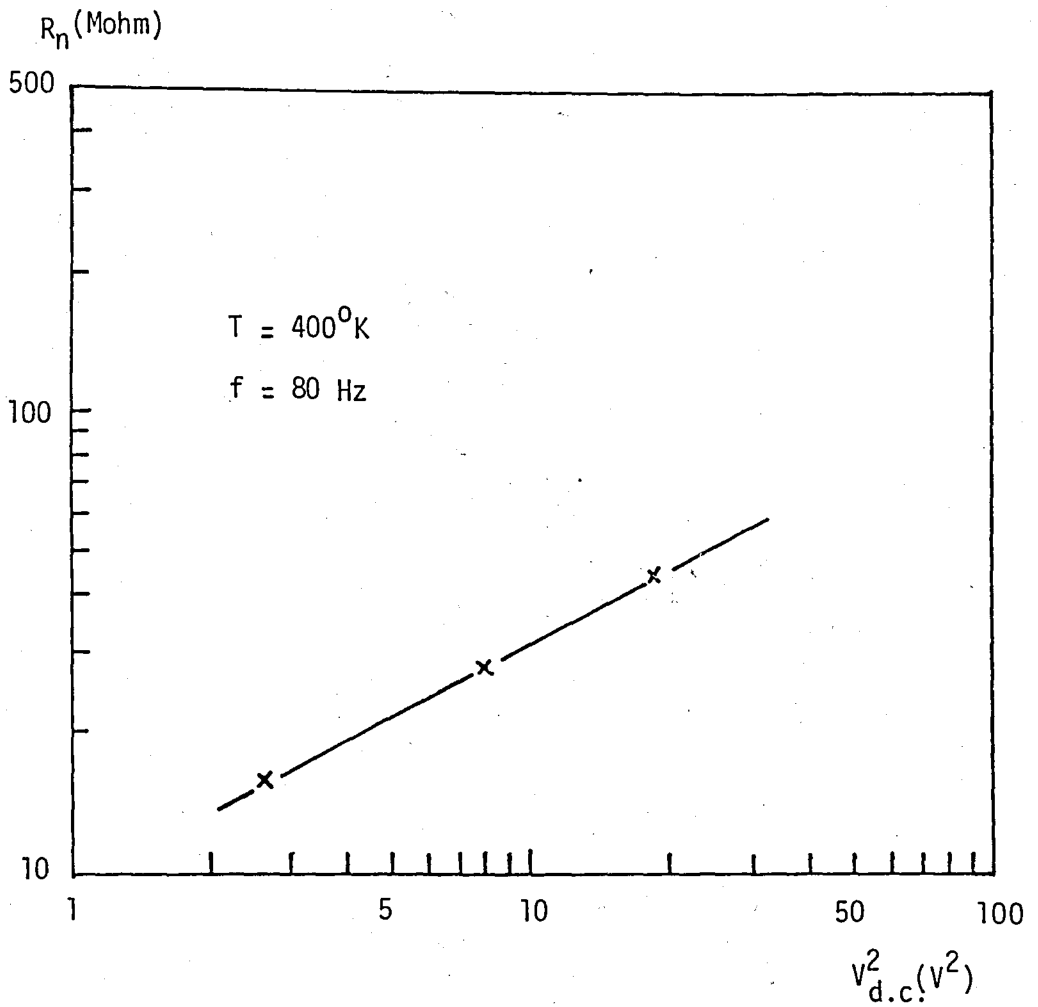

FIGURE 3.18. Effective Noise Resistance versus $V^2_{d.c.}$ Graph at High Temperature

CHAPTER IV

CONCLUSIONS

Measurements performed on both coplanar and sandwich type amorphous silicon films have shown that, the low-frequency noise is basically due to 1/f type fluctuations at room temperature.

Since the dominant mechanism of conduction at room temperature is phonon assisted hopping, the 1/f noise is expected to have frequency spectra similar to those of hopping rate fluctuations, as verified experimentally.

The density of states at Fermi level $N(E_F)$ can be determined from the 1/f noise measurements by means of Hooge's empirical formula. It is therefore possible to study some of the electronic properties of amorphous silicon using low-frequency noise measurements.

When compared with the crystalline silicon samples, amorphous ones are measured to be noisier.

Low-frequency noise measurements are extended to higher temperatures ($440^{0}K$) and noise level is found to decrease with temperature;

the power spectrum rather follows a $1/f^{1.5}$ shape.

In the high temperature range, the conductivity mechanism involved is band-to-band, quite similar to the conduction in crystalline structure.

Temperature dependence of noise in amorphous silicon seems to be another topic of interest for future studies.

REFERENCES

[1] ADLER, David, Amorphous Semiconductors, CRC Press, Ohio, 1971.

[2] YONEZAWA, Fumiko, Fundamental Physics of Amorphous Semiconductors, Springer, Grünstadt, 1981.

[3] ELLIOT, S.R., "Defect States in Amorphous Silicon," Philosophical Magazine B., Vol. 38, No.4, pp. 325-334, 1978.

[4] ATAĞ, Yılmaz, "Study of the D.C. Conductance Mechanism of Evaporated Silicon Films", M.S. Thesis, Boğaziçi University, 1984.

[5] MOTT, N.F. and DAVIS, E.A., Electronic Processes in Non-Crystalline Materials, Oxford, Clarenden Press, 1979.

[6] COHEN, M.H., FRITZSHE, H. and OVSHINSKY, S.K., "Simple Band Model for Amorphous Semiconducting Alloys", Phys. Rev. Letters, Vol. 22, No.2, pp. 1065-1068, 1969.

[7] STUKE, J. and BRENIG, W., Amorphous and Liquid Semiconductors, Taylor-Francis Ltd., London, 1974.

[8] TAUC, J., Amorphous and Liquid Semiconductors, Plenum Press, 1974.

[9] LECOMBER, P.G., Electronic and Structural Properties of Amorphous Semiconductors, London, Academic Press, 1972.

[10] D'AMICO, A. and FORTUNATO, G., "Conductivity and Noise in Thin Films of Nonhydrogenated Amorphous Silicon in the Hopping Regime," Solid State Electronics, Vol. 28, No.8, pp. 837-844, 1985.

[11] ÜLGEN, Yekta, "Low-Frequency Noise in Resistors Excited By Various Current Waveforms", Ph.D. Thesis, University of Salford, 1978.

[12] ÜLGEN, Yekta, Theory of Narrow-Band Noise Detection, Boğaziçi University, Istanbul, 1983.

[13] HOOGE, F.N., "Discussion of Recent Experiments on 1/f Noise", Physica, Vol. 60, pp. 130-144, 1972.

[14] VANDERZIEL, A., Noise: Source, Characterization, Measurement, Prentice-Hall Inc., New Jersey, 1970.

[15] AMBROZY, Á., Electronic Noise, Mc.Graw Hill, Budapest, 1982.

[16] VANDERZIEL, A., Noise in Solid State Devices and Circuits, John Wiley and Sons, New York, 1986.

[17] MOTCHENBACHER, C.D. and FITCHEN, F.C., Low-noise Electronic Design, John Wiley and Sons, 1977.

[18] MARSHALL, I. and BRYDON, J., "Semiconductor Noise Analyser", Wireless Word, May, 1983.

[19] BLACK, R.D., WEISMANN, M.B. and RESTLE, P.J., "1/f Noise in Silicon Wafers," J.Appl. Phys., Vol. 53, No. 9, pp. 6280-6284, 1982.

[20] BATHAEI, F.Z. and ANDERSON, J.C., "Electrical Noise Measurements in Intrinsic Amorphous Silicon", Philosophical Magazine B., Vol. 55, No. 1, pp. 87-100, 1986.